MIT Libraries | DSpace@MIT

MIT Open Access Articles

AN ANALYTICAL MODEL OF THE LARGE NEUTRAL REGIONS DURING THE LATE STAGE OF REIONIZATION

The MIT Faculty has made this article openly available. ***Please share*** how this access benefits you. Your story matters.

Citation: Xu, Yidong, Bin Yue, Meng Su, Zuhui Fan, and Xuelei Chen. "AN ANALYTICAL MODEL OF THE LARGE NEUTRAL REGIONS DURING THE LATE STAGE OF REIONIZATION." The Astrophysical Journal 781, no. 2 (January 14, 2014): 97. © 2014 American Astronomical Society.

As Published: http://dx.doi.org/10.1088/0004-637x/781/2/97

Publisher: Institute of Physics/American Astronomical Society

Persistent URL: http://hdl.handle.net/1721.1/92914

Version: Final published version: final published article, as it appeared in a journal, conference proceedings, or other formally published context

Terms of Use: Article is made available in accordance with the publisher's policy and may be subject to US copyright law. Please refer to the publisher's site for terms of use.

Massachusetts Institute of Technology

The Astrophysical Journal, 781:97 (15pp), 2014 February 1 doi:10.1088/0004-637X/781/2/97
© 2014. The American Astronomical Society. All rights reserved. Printed in the U.S.A.

AN ANALYTICAL MODEL OF THE LARGE NEUTRAL REGIONS DURING THE LATE STAGE OF REIONIZATION

Yidong Xu[1], Bin Yue[1], Meng Su[2,3,6], Zuhui Fan[4], and Xuelei Chen[1,5]
[1] National Astronomical Observatories, Chinese Academy of Sciences, Beijing 100012, China
[2] Department of Physics, and Kavli Institute for Astrophysics and Space Research, Massachusetts Institute of Technology, Cambridge, MA 02139, USA
[3] Institute for Theory and Computation, Harvard-Smithsonian Center for Astrophysics, 60 Garden Street, MS-51, Cambridge, MA 02138, USA
[4] Department of Astronomy, Peking University, Beijing 100871, China
[5] Center for High Energy Physics, Peking University, Beijing 100871, China
Received 2013 June 21; accepted 2013 December 16; published 2014 January 14

ABSTRACT

In this paper, we investigate the nature and distribution of large neutral regions during the late epoch of reionization. In the "bubble model" of reionization, the mass distribution of large ionized regions ("bubbles") during the early stage of reionization is obtained by using the excursion set model, where the ionization of a region corresponds to the first up-crossing of a barrier by random trajectories. We generalize this idea and develop a method to predict the distribution of large-scale neutral regions during the late stage of reionization, taking into account the ionizing background after the percolation of H II regions. The large-scale neutral regions, which we call "neutral islands," are not individual galaxies or minihalos, but larger regions where fewer galaxies formed and hence ionized later and they are identified in the excursion set model with the first down-crossings of the island barrier. Assuming that the consumption rate of ionizing background photons is proportional to the surface area of the neutral islands, we obtained the size distribution of the neutral islands. We also take the "bubbles-in-island" effect into account by considering the conditional probability of up-crossing a bubble barrier after down-crossing the island barrier. We find that this effect is very important. An additional barrier is set to avoid islands being percolated through. We find that there is a characteristic scale for the neutral islands, while the small islands are rapidly swallowed up by the ionizing background; this characteristic scale does not change much as the reionization proceeds.

Key words: cosmology: theory – dark ages, reionization, first stars – intergalactic medium – large-scale structure of universe – methods: analytical

Online-only material: color figures

1. INTRODUCTION

Cosmic reionization is one of the most important but poorly understood epochs in the history of the universe. As the first stars form in the earliest non-linear structures, they illuminate the ambient intergalactic medium (IGM), create H II regions around them, and start the reionization process of hydrogen. As the sources become brighter and more numerous, H II regions grow in number and size, then merge with each other and eventually percolate throughout the IGM. Various observations have put constraints on the reionization process. Based on an instantaneous reionization model, the temperature and polarization data of the cosmic microwave background constrain the redshift of reionization to be $z_{\rm reion} = 11.1 \pm 1.1$ (1σ; Planck Collaboration et al. 2013a), while the absence of Gunn–Peterson troughs (Gunn & Peterson 1965) in high-redshift quasar absorption spectra suggest that the reionization of hydrogen was very nearly complete by $z \approx 6$ (e.g., Fan et al. 2006). Several deep extragalactic surveys have found more than 200 galaxies at $z \sim 7$–8, but these are still the tip of the iceberg, i.e., the most luminous of the galaxy population at those redshifts (e.g., Bouwens et al. 2011; Oesch et al. 2012; McLure et al. 2013; Schenker et al. 2012; Lorenzoni et al. 2013; Bradley et al. 2012; Finkelstein et al. 2012). Recently, measurements of the kinetic Sunyaev–Zel'dovich effect with the South Pole Telescope have been used to put limits on the epoch and duration of reionization (Mesinger et al. 2012; Zahn et al. 2012; Battaglia et al. 2012a), although the obtained limits depend on the detailed physics of reionization (Zahn et al. 2012; Park et al. 2013).

The most promising probe of this evolutionary stage is the 21 cm transition of neutral hydrogen (see Furlanetto et al. 2006 for a review). The EDGES[7] experiment has put the first observational lower limit on the duration of the epoch of reionization of $\Delta z > 0.06$ (Bowman & Rogers 2010) and using the GMRT,[8] Paciga et al. (2011, 2013) put upper limits on the neutral hydrogen power spectrum. The upcoming low-frequency interferometers such as LOFAR,[9] PAPER,[10] MWA,[11] and 21CMA[12] may be able to detect signatures of reionization and next-generation instruments such as HERA[13] and SKA[14] may be able to map out the reionization process in more detail and reveal the properties of the first luminous objects. Interpreting the upcoming data from these instruments requires detailed modeling of the reionization process.

[6] Einstein Fellow

[7] Experiment to Detect the Global EoR Signature; see http://www.haystack.mit.edu/ast/arrays/Edges/
[8] The Giant Metrewave Radio Telescope; see http://gmrt.ncra.tifr.res.in/
[9] The Low Frequency Array; see http://www.lofar.org/
[10] The Precision Array for Probing the Epoch of Reionization; see http://eor.berkeley.edu/
[11] The Murchison Widefield Array; see http://www.mwatelescope.org/
[12] The 21 Centimeter Array; see http://21cma.bao.ac.cn/
[13] The Hydrogen Epoch of Reionization Array; see http://reionization.org/
[14] The Square Kilometre Array; see http://www.skatelescope.org/

Motivated by the results of numerical simulations, Furlanetto et al. (2004) developed a "bubble model" for the growth of H II regions during the early reionization era. In this model, at a given moment during the early stage of reionization, a region is assumed to be ionized if the total number of ionizing photons produced within exceeds the average number required to ionize all the hydrogen in the region. Otherwise, it is assumed to be neutral, although there could be smaller H II regions within it. At the very beginning, the ionized regions are mostly the surroundings of the just-formed first stars or galaxies, but as the high-density regions where first stars and galaxies formed are strongly correlated, very soon these regions would grow larger and merge to contain several nearby galaxies. The bubble model treatment can deal with the fact that a region can be ionized by neighboring sources rather than only interior galaxies.

In the bubble model, the number of star-forming halos and ionizing photons are calculated with the extended Press–Schechter model (Bond et al. 1991; Lacey & Cole 1993). The criterion of ionization is equivalent to the condition that the average density of the region exceeds a certain threshold value (ionization barrier). The mass function of the H II region can then be obtained from the excursion set model, i.e., by calculating the probability of a random walk trajectory first upcrossing the barrier. With a linear fit to the ionization barrier, Furlanetto et al. (2004) obtained the H II bubble mass function during the early stage of reionization (see the next section for more details). This analytical model matches simulation results reasonably well (Zahn et al. 2007) and is much faster to compute than the radiative transfer numerical simulations, so it can be used to explore a large parameter space. It also provides us with an intuitive understanding of the physics of the reionization process. Instead of the full analytical calculation, one can also apply the same idea to make semi-numerical simulations (Zahn et al. 2007; Mesinger & Furlanetto 2007; Alvarez et al. 2009; Choudhury et al. 2009; Zhou et al. 2013). In these simulations, the density field is generated by the usual *N*-body simulation or the first-order perturbation theory and the ionization field is then predicted with the same criteria as the analytical model. The semi-numerical approach allows relatively fast computation, while at the same time providing three-dimensional visualization of the reionization process.

The bubble model also has certain limitations. As H II regions form and grow, they begin to contact with each other and spherical "bubbles" are no longer a good description of the H II regions. After percolation of the H II regions, the photons from more distant regions, i.e., the ionizing background, become very important. Eventually, the total volume fraction of the bubbles predicted by the model would exceed one and slightly before this moment the bubble model breaks down. Although the bubble model may still be successful in some average sense after percolation and Zahn et al. (2007) indeed obtained fairly good agreement between the model-based semi-numerical simulation and radiative transfer simulations even after ionized bubbles overlap, it is necessary to construct a more accurate model for the late stage of reionization to account for the non-bubble topology and the existence of an ionizing background.

One may use similar reasonings to construct an analytical model for the remaining neutral regions after the percolation of ionized regions. During this epoch, the high density of galaxies and minihalos allows them to have a higher recombination rate and thus remain neutral. Besides these compact neutral regions, there are also large regions with relatively low density, which remain neutral because fewer galaxies formed within them. We shall call these neutral regions "islands," which remain above the flooding ionization for a moment. This is in some sense similar to the voids of large-scale structure; just as the extended Press–Schechter model can predict the number of both halos and voids, we can also develop models of the neutral islands. However, we do need to change the barrier to take into account the background ionizing photons in order to model the island evolution correctly.

On the observational side, the island distribution and its evolution are important for the 21 cm signal, which directly relates to the neutral components in the universe, and it would be relatively easier upcoming instruments to probe the signal at the late reionization stages, where the redshifted 21 cm lines have higher frequencies and weaker foregrounds. Also, the neutral islands may also contribute to the overall opacity of the IGM in addition to the Lyman limit systems (LLSs) and in turn affect the evolution of the ultraviolet background and the detectability of high-redshift galaxies (e.g., Bolton & Haehnelt 2013).

In this paper, we aim to construct an analytical island model that is complementary to the bubble model. It applies to the neutral regions left over after the ionized bubbles overlap with each other, when the neutral islands are more isolated. Based on the excursion set formalism, we identify the islands by finding the first crossings of the random walks downward the island barrier, which are deeper than the bubble barrier because they take into account the background ionizing photons in addition to the photons produced by stars inside the island region. We then use the excursion set model to calculate the crossing probability at different mass scales and derive the mass distribution function of the islands.

However, inside the large neutral islands smaller ionized bubbles may also form. We investigate this "bubbles-in-island" problem by considering the conditional probability for the excursion trajectory to first down-cross the island barrier, then up-cross the original bubble barrier (without the contribution of the ionizing background) at a smaller scale. It turns out that a large number of bubbles may form inside the islands, such that a large fraction of the insides of some "islands" are ionized. However, we may set a percolation threshold as an upper limit on the "bubbles-in-island" fraction, below which the islands are still relatively simple. We also try to shed light on the shrinking process of the islands and obtain a coherent picture of the late stage of the epoch of reionization.

In the following, we first briefly review the excursion set theory and the bubble model in Section 2, then we generalize it and develop the formalism of the "island model" in Section 3; we employ a simple toy model to illustrate the calculation. An important aspect of the theory is the treatment of the so-called bubbles-in-island problem, i.e., self-ionized bubbles inside the neutral islands. We also discuss how to take this effect into account. Section 4 presents our treatment of the ionizing background taking into account absorption from LLSs. With these tools in hand, we study the reionization process in Section 5; the consumption rate of background ionizing photons is assumed to be proportional to the surface area of the island. The size distribution of the islands is calculated for different redshifts. We summarize our results and conclude in Section 6. Throughout this paper, we adopt the cosmological parameters from the 7 yr *Wilkinson Microwave Anisotropy Probe* measurements combined with baryon acoustic oscillation and H_0 data: $\Omega_b = 0.0455$, $\Omega_c = 0.227$, $\Omega_\Lambda = 0.728$, $H_0 = 70.2\,\mathrm{km\,s^{-1}\,Mpc^{-1}}$, $\sigma_8 = 0.807$, and $n_s = 0.961$

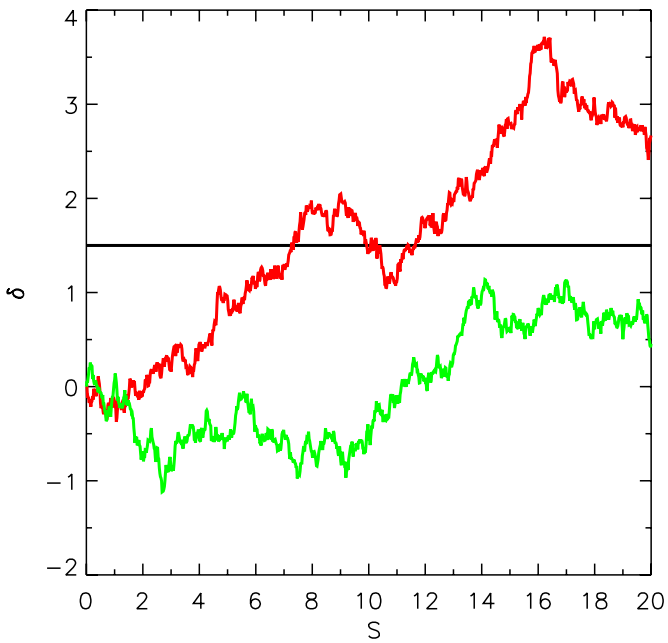

Figure 1. Two random walk trajectories in the excursion set theory. Here, $S = \sigma^2(M)$ denotes the variance of $\delta_{\rm M}$, which is the density fluctuation smoothed on a mass scale M. All trajectories originate from $(S, \delta) = (0, 0)$. The horizontal line represents a flat barrier, motivated by spherical collapse.

(A color version of this figure is available in the online journal.)

(Komatsu et al. 2011), but the results are not sensitive to these parameters.

2. A BRIEF REVIEW OF THE EXCURSION SET THEORY AND THE BUBBLE MODEL

2.1. The Excursion Set Model

Our island model is based on the excursion set theory. Here, we give a brief review of the excursion set approach, especially its application to the reionization process, i.e., the bubble model. For a more comprehensive review of the excursion set theory and its extensions and applications, we refer interested readers to Zentner (2007) and references therein.

In what follows, we consider the density contrast field evaluated at some early time but extrapolated to the present day using linear perturbation theory. Considering a point $\mathbf{x}$ in space, the density contrast $\delta(\mathbf{x})$ around it depends on the smooth mass scale M under consideration. The variance of the density fluctuations on a scale M, $S = \sigma^2(M)$, monotonically decreases with increasing M in our universe, so we can use S to represent the scale M. Starting at $M = \infty$, i.e., $S = 0$, we move to smaller and smaller scales surrounding the point of interest and compute the smoothed density field as we go along. If we use a k-space tophat window function to smooth the density field, at each scale k a set of independent Fourier modes are added and the trajectory of δ can be described by a random walk where each step is independent, forming random trajectories on the S–δ plane. Each of these trajectories starts from the origin of the (S, δ) plane, with the variance of all trajectories given by $\langle \delta^2(S) \rangle = S$. Two sample trajectories are shown in Figure 1. Typically, the trajectories jitter more and deviate farther from $\delta = 0$ at larger S.

It is assumed that at redshift z and on scale M, regions with an average density above a certain threshold value δ_c will collapse into halos, while regions with an average density below the threshold would remain uncollapsed. The galaxies form inside sufficiently massive halos. In some models, δ_c is only a function of redshift; more generally, it is a function of both redshift and mass scale. The formation of a halo corresponds to the trajectory up-crossing a barrier $\delta_c(M, z)$ in the S–δ plane. The excursion set theory was developed to compute the probabilities for such crossing and gives the mass distribution of the corresponding halos.

An important issue that must be addressed is the "cloud-in-cloud" problem. For a given central point, the critical threshold could be exceeded multiple times, corresponding to possible halos on different mass scales. In the excursion set theory, one determines the largest smoothing scale M (smallest S) at which a trajectory first up-crosses the halo barrier at δ_c and identify it as the halo at that redshift, while smaller-scale crossings are ignored. Physically, it is reasonable to think that the smaller-scale upcrossing corresponds to a small halo that formed earlier and merged into the larger halo.

The probability of the barrier crossing can be computed by solving a diffusion equation with the appropriate boundary conditions and the first crossing probability can be calculated with an absorbing barrier. For a constant density barrier and a starting point of (δ_0, S_0), the differential probability of first-crossing of the barrier δ_c at S, known as the "first-crossing distribution," can be written as

$$f(S|\delta_0, S_0)dS = \frac{\delta_c - \delta_0}{\sqrt{2\pi}(S - S_0)^{3/2}} \exp\left[-\frac{(\delta_c - \delta_0)^2}{2(S - S_0)}\right] dS \tag{1}$$

and around the whole universe, the mass function of the virialized halos is obtained by setting $S_0 = 0$ and $\delta_0 = 0$, which is

$$\frac{dn}{d\ln M} = \bar{\rho}_{\rm m,0} f(S) \left|\frac{dS}{dM}\right|. \tag{2}$$

Besides the halo mass function, the excursion set theory can also be used to model the halo formation and growth (Bond et al. 1991; Lacey & Cole 1993) and halo clustering properties (Mo & White 1996). Apart from the virialized halos, it could be applied to various structures in the universe, such as the voids in the galaxy distribution (Sheth & van de Weygaert 2004; Paranjape et al. 2012a; Furlanetto & Piran 2006; D'Aloisio & Furlanetto 2007) and the ionized bubbles during the early stages of reionization (Furlanetto et al. 2004). It has also been extended to the case of moving barriers (Sheth & Tormen 2002; Zhang & Hui 2006). Strictly speaking, the probabilities given above are calculated for uncorrelated steps, which is correct for the k-space tophat filter but not for the real-space tophat filter. An excursion set model with correlated steps has also been developed (Pan et al. 2008; Paranjape et al. 2012b; Paranjape & Sheth 2012; Musso & Sheth 2012; Farahi & Benson 2013; Musso & Sheth 2013), but below we will still use the uncorrelated model for its simplicity.

2.2. The Bubble Model

In the excursion set model of ionized bubbles during reionization, i.e., the "bubble model," a region is considered ionized if it could emit sufficient ionizing photons to ionize all of the hydrogen atoms in the region (Furlanetto et al. 2004). Assuming that the number of the ionizing photons emitted is proportional to the total collapse fraction of the region, the ionization condition can be written as

$$f_{\rm coll} \geqslant \xi^{-1}, \tag{3}$$

where

$$\xi = f_{\rm esc}\, f_\star\, N_{\gamma/{\rm H}}\,(1+\bar{n}_{\rm rec})^{-1} \tag{4}$$

is an ionizing efficiency factor, in which $f_{\rm esc}$, $f_\star$, $N_{\gamma/{\rm H}}$, and $\bar{n}_{\rm rec}$ are the escape fraction, star-formation efficiency, the number of ionizing photons emitted per H atom in stars, and the average number of recombinations per ionized hydrogen atom, respectively. For a Gaussian density field, the collapse fraction of a mass scale M with the mean linear overdensity $\delta_{\rm M}$ at redshift z can be written as (Bond et al. 1991; Lacey & Cole 1993)

$$f_{\rm coll}(\delta_{\rm M}; M, z) = {\rm erfc}\left[\frac{\delta_c(z)-\delta_{\rm M}}{\sqrt{2[S_{\rm max}-S(M)]}}\right], \tag{5}$$

where $S_{\rm max} = \sigma^2(M_{\rm min})$, in which $M_{\rm min}$ is the minimum collapse scale, and $\delta_c(z)$ is the critical density for collapse at redshift z linearly extrapolated to the present time. $M_{\rm min}$ is usually taken to be the mass corresponding to a virial temperature of 10^4 K, at which atomic hydrogen line cooling becomes efficient. With this collapse fraction, the self-ionization constraint can be written as a barrier on the density contrast (Furlanetto et al. 2004):

$$\delta_{\rm M} > \delta_{\rm B}(M,z) \equiv \delta_c(z) - \sqrt{2[S_{\rm max}-S(M)]}\,{\rm erfc}^{-1}(\xi^{-1}). \tag{6}$$

Solving for the first-up-crossing distribution of random walks with respect to this barrier, $f(S,z)$, the bubbles-in-bubble effect has been included and the size distribution of ionized bubbles can be obtained from Equation (2) and then the average volume fraction of ionized regions can be written as

$$Q_{\rm V}^{\rm B} = \int dM\,\frac{dn}{dM}\,V(M). \tag{7}$$

In the linear approximate solution, $\delta_{\rm B}(M,z) = \delta_{\rm B,0} + \delta_{\rm B,1} S$, with the intercept of the $S=0$ axis given by

$$\delta_{\rm B,0} \equiv \delta_c(z) - \sqrt{2\,S_{\rm max}}\,{\rm erfc}^{-1}(\xi^{-1}), \tag{8}$$

and the slope is

$$\delta_{\rm B,1} \equiv \left.\frac{\partial\delta_{\rm B}}{\partial S}\right|_{S\to 0} = \frac{{\rm erfc}^{-1}(\xi^{-1})}{\sqrt{2S_{\rm max}}}. \tag{9}$$

The number density of H II bubbles is then given by (Furlanetto et al. 2004):

$$M\frac{dn}{dM} = \frac{1}{\sqrt{2\pi}}\,\bar{\rho}_{\rm m,0}\left|\frac{dS}{dM}\right|\frac{\delta_{\rm B,0}}{S^{3/2}}\exp\left[-\frac{\delta_{\rm B}^2(M,z)}{2\,S}\right]. \tag{10}$$

According to the bubble model, at high redshifts the regions of high overdensity were ionized earlier, because only in such regions were galaxy-harboring halos formed, producing sufficient number of ionizing photons. In the excursion set theory, this is represented by those trajectories that excurse over the high barrier $\delta_{\rm B}(S)$. As structures grow, the barrier function $\delta_{\rm B}(S)$ decreases and thus regions of relatively lower density become ionized. As the density and size of bubbles increase, they begin to overlap. As long as the topology of the bubbles remains mostly discrete, this description is valid. However, at a certain point, the intercept $\delta_{\rm B,0}$ drops low enough to 0 that all trajectories that started out growing from the origin point of the S–δ plane would have crossed the barrier and regions of the average density of the universe would have been ionized. In fact, the bubble description of H II regions perhaps failed slightly earlier, because when the ionized regions occupy a sizable fraction of the total volume, they become connected, the topology becomes sponge-like, and it is no longer possible to treat the ionized regions as individual bubbles.

3. THE EXCURSION SET MODEL OF NEUTRAL ISLANDS

3.1. The General Formalism

The bubble model succeeds in describing the growth of H II regions before the percolation of H II regions. As a natural generalization to the bubble model, we develop a model that is appropriate for the late stage of reionization, when the H II regions have overlapped with each other and the neutral regions are more isolated and embedded in the sea of photon-ionized plasma and ionizing photons. According to the bubble model, the regions with higher densities are ionized earlier and by this stage even the regions of average density have been ionized, so the remaining large-scale neutral regions ("islands") are underdense regions. Of course, besides these large neutral regions, there are also galaxies and minihalos, in which neutral hydrogen exists because they have very high density and hence high recombination rates, which keep them from being ionized. We shall not discuss these small, highly dense H I systems in this paper; their number distribution can be predicted with the usual halo model formalism (see Cooray & Sheth 2002 for a review). The neutral islands during the late era of reionization are more likely isolated than the ionized bubbles, similar to the voids at lower redshifts.

In the island model, we assume that most of the universe has been ionized, but the reionization has not been completed. The condition for a region to remain neutral is just the opposite of the ionization condition, that is, the total number of ionizing photons is fewer than the number required to ionize all hydrogen atoms in the region. At this stage, however, it is also important to include the background ionizing photons that are produced outside the region. An island of mass scale M at redshift z has to satisfy the following condition in order to remain neutral:

$$\xi f_{\rm coll}(\delta_{\rm M}; M, z) + \frac{\Omega_m}{\Omega_b}\frac{N_{\rm back} m_{\rm H}}{M X_{\rm H}(1+\bar{n}_{\rm rec})} < 1, \tag{11}$$

where $N_{\rm back}$ is the number of background ionizing photons that are consumed by the island and $X_{\rm H}$ is the mass fraction of the baryons in hydrogen. The first term on the left-hand side is due to self-ionization, while the second term is due to the ionizing background. Note that in the usual convention of the bubble model, the number of the recombination factor $(1+\bar{n}_{\rm rec})^{-1}$ is absorbed in the ξ parameter and, to be consistent with the literature, here we follow this convention. However, we should keep in mind that if one changes $\bar{n}_{\rm rec}$, the adopted ξ value should be changed accordingly.

Using Equation (5), the condition of Equation (11) can be rewritten as a constraint on the overdensity of the region:

$$\delta_{\rm M} < \delta_{\rm I}(M,z) \equiv \delta_c(z) - \sqrt{2[S_{\rm max}-S(M)]}\,{\rm erfc}^{-1}[K(M,z)], \tag{12}$$

where

$$K(M,z) = \xi^{-1}\left[1 - N_{\rm back}(1+\bar{n}_{\rm rec})^{-1}\frac{m_{\rm H}}{M(\Omega_b/\Omega_m)X_{\rm H}}\right]. \tag{13}$$

Due to the contribution of the ionizing background photons, in the excursion set model the barrier for the neutral islands is different from the barrier used in the bubble model (Equation (6)), as the ionizing background would not be present when the bubbles are isolated. Below, we refer to a barrier with only the

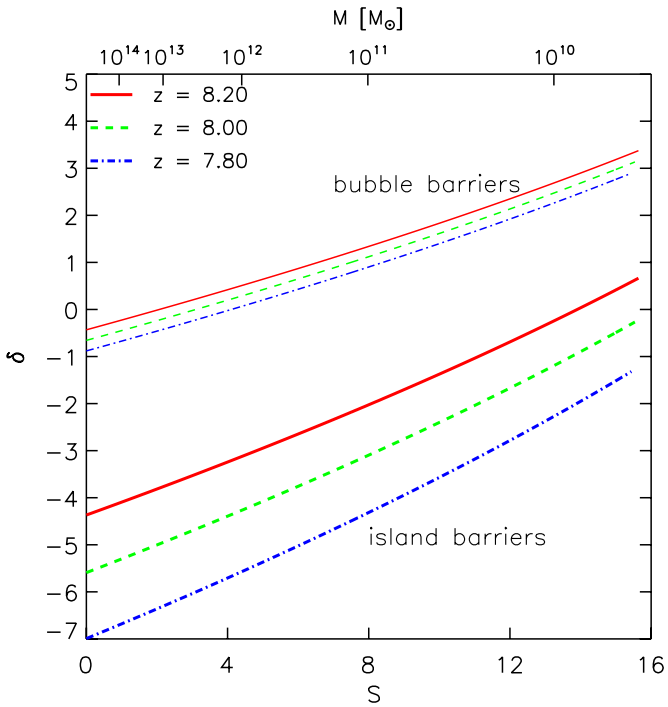

Figure 2. Island barriers in the model with uniform island-permeating ionizing background photons. The barriers are plotted for redshifts 8.2, 8.0, and 7.8 as thick curves, from top to bottom, respectively. Here, we assume $\{f_{\rm esc}, f_\star, N_{\gamma/H},$ and $\bar{n}_{\rm rec}\} = \{0.2, 0.1, 4000, 1\}$. The bubble barriers (without ionizing background) at the same set of redshifts are shown as thin curves. On the top of the figure box, we also show the mass scales corresponding to S for reference.

(A color version of this figure is available in the online journal.)

self-ionization term the "bubble barrier," denoted by $\delta_{\rm B}(M, z)$, since it is used to compute the probability of forming bubbles. Inclusion of the ionizing background would make the barrier much more negative and we refer to the full barrier as the "island barrier," denoted by $\delta_{\rm I}(M, z)$.

As discussed in the last section, the bubble barrier hinders progress of structure formation. Even if we simply compute the barrier as in the original bubble model, i.e., including only the ionizing photons from collapsed halos within the region being considered, it could have negative intercepts, i.e., $\delta_{\rm B}(S = 0) < 0$ (see, e.g., the thin lines in Figure 2). When the bubble barrier passes through the origin point of the δ–S plane, all regions with the mean density $\delta = 0$ are ionized, meaning that most of the universe is ionized. It is also from this moment onward that a global ionizing background is gradually set up. We define the redshift when this occurred as the "background onset redshift" $z_{\rm back}$ and it can be solved for from the following equation:

$$\delta_{\rm I}(S = 0; z = z_{\rm back}) = \delta_c(z_{\rm back}) - \sqrt{2\, S_{\rm max}(z_{\rm back})}\, {\rm erfc}^{-1}(\xi^{-1}) = 0. \quad (14)$$

We take $\{f_{\rm esc}, f_\star, N_{\gamma/\rm H},$ and $\bar{n}_{\rm rec}\} = \{0.2, 0.1, 4000, 1\}$ as the fiducial set of parameters, so that $\xi = 40$ and $z_{\rm back} = 8.6$, consistent with the observations of the quasar/gamma-ray burst absorption spectra (Gallerani et al. 2008a, 2008b) and Lyman-α emitter surveys (e.g., Malhotra & Rhoads 2006; Dawson et al. 2007), which suggest $x_{\rm H\,I} \ll 1$ at $z \approx 6$. We note that this background onset redshift is also consistent with our ionizing background model presented in Section 4, in which the intensity of the ionizing background starts to rapidly increase around redshift $z \sim 8$–9 (see Figure 5). However, the exact value of this background onset redshift has little impact on the final model predictions on the island distribution, as the ionizing background increases quite rapidly during the late stage of reionization (see Section 4) and the main background contribution to the ionizations comes from the redshift range just above the redshift under consideration.

As all trajectories start from the point $(S, \delta) = (0, 0)$ and the island barrier has a negative intercept, we see that instead of the usual up-crossing condition in the excursion set model, here the condition of forming a neutral island is represented by a down-crossing of the barrier. Once a random walk trajectory hits the island barrier, we identify an island with the crossing scale and assign the points inside this region to a neutral island of the appropriate mass. Similar to the "cloud-in-cloud" problem in the halo model (Bond et al. 1991) or the "void-in-void" problem in the void model (Sheth & van de Weygaert 2004), there is also an "island-in-island" problem. As in those cases, this problem can also be solved naturally by considering only the first down-crossings of the barrier curve.

For a general barrier, Zhang & Hui (2006) developed an integral equation method for computing the first up-crossing distribution. Similarly, denoting the island scale with its variance $S_{\rm I}$, the first down-crossing distribution of random trajectories with an arbitrary island barrier can be solved as

$$f_{\rm I}(S_{\rm I}) = -g_1(S_{\rm I}) - \int_0^{S_{\rm I}} dS'\, f_{\rm I}(S')[g_2(S_{\rm I}, S')], \quad (15)$$

where

$$g_1(S_{\rm I}) = \left[\frac{\delta_{\rm I}(S_{\rm I})}{S_{\rm I}} - 2\frac{d\delta_{\rm I}}{dS_{\rm I}}\right] P_0[\delta_{\rm I}(S_{\rm I}), S_{\rm I}], \quad (16)$$

$$g_2(S_{\rm I}, S') = \left[2\frac{d\delta_{\rm I}}{dS_{\rm I}} - \frac{\delta_{\rm I}(S_{\rm I}) - \delta_{\rm I}(S')}{S_{\rm I} - S'}\right] \times P_0[\delta_{\rm I}(S_{\rm I}) - \delta_{\rm I}(S'), S_{\rm I} - S'], \quad (17)$$

and $P_0(\delta, S)$ is the normal Gaussian distribution with variance S, which is defined as

$$P_0(\delta, S) = \frac{1}{\sqrt{2\pi S}} \exp\left(-\frac{\delta^2}{2S}\right). \quad (18)$$

These integral equations can be solved numerically with the algorithm of Zhang & Hui (2006). We can then obtain the mass function of islands at redshift z:

$$\frac{dn}{d\ln M_{\rm I}}(M_{\rm I}, z) = \bar{\rho}_{\rm m,0} f_{\rm I}(S_{\rm I}, z) \left|\frac{dS_{\rm I}}{dM_{\rm I}}\right|. \quad (19)$$

With the neutral island mass function, the volume fraction of neutral regions is given by

$$Q_{\rm V}^{\rm I} = \int dM_{\rm I}\, \frac{dn}{dM_{\rm I}}\, V(M_{\rm I}). \quad (20)$$

3.2. A Toy Model with Island-permeating Ionizing Background Photons

To illustrate the basic ideas of the island model, let us consider a toy model in which the ionizing photons permeated through the neutral islands with a uniform density. This is not a physically realistic model, because if ionizing photons

can permeate through the neutral regions with sufficient flux there would be no distinct ionizing bubbles or neutral islands, although it may be possible to have a small component of penetrating radiation such as hard X-rays, but that would be much smaller than the total ionizing background. The reason we consider this model is that it is possible to derive a simple analytical solution, which could illustrate some aspects of the island model.

The island-permeating ionizing background photons are likely to be hard X-rays, whose mean free paths are extremely large even in an IGM with a high neutral fraction. Therefore, we use here an extremely simple model for the ionizing background, in which the absorptions by dense clumps are neglected and the mean free path of these background photons is comparable with the Hubble scale. In any case, this is a toy model; a more realistic model for the ionizing background will be described in the next section. Furthermore, we assume that the total number of ionizing photons produced by redshift z is proportional to the total collapse fraction of the universe at that redshift. Some of these photons would have already been consumed by ionizations took place before that redshift and the ionizing background photons are what were left behind. The comoving number density of background ionizing photons is then given by

$$n_\gamma = \bar{n}_{\rm H}\, f_{\rm coll}(z)\, f_\star\, N_{\gamma/{\rm H}}\, f_{\rm esc} - \left(1 - Q_{\rm V}^{\rm I}\right) \bar{n}_{\rm H}\,(1 + \bar{n}_{\rm rec}), \quad (21)$$

where $\bar{n}_{\rm H}$ is the average comoving number density of hydrogen in the universe and the other parameters are the same as those in Equation (3). The number density of ionizing photons given by Equation (21) depends on the global neutral fraction $Q_{\rm V}^{\rm I}$, which is only known after we have applied the ionizing background intensity itself and solved the reionization model, so this equation should be solved iteratively.

Supposing that the background ionizing photons are uniformly distributed and consumed within the islands, then $N_{\rm back}$ is proportional to the island volume. We see from Equation (13) that $N_{\rm back}$ cancels with the island mass M in the denominator and we have $N_{\rm back}/M = n_\gamma/\bar{\rho}_{\rm m}$. Therefore, in this model, the K factor is essentially independent of M, i.e., $K(M, z) = K(z)$. Then, the island barrier becomes:

$$\delta_{\rm I}(M, z) = \delta_c(z) - \sqrt{2\,[S_{\rm max} - S(M)]}\,{\rm erfc}^{-1}[K(z)]. \quad (22)$$

For a given redshift, K = constant, so, similarly to the bubble barrier, the only dependence of the island barrier on mass scale comes from $S(M)$. Taking the fiducial set of parameters, we plot the island barriers at redshifts 8.2, 8.0, and 7.8 in Figure 2 with thick curves, from top to bottom, respectively. The bubble barriers are also plotted with thin lines in the same figure. Indeed, in this case, the island barriers have a similar shape as the bubble barriers. Both barriers increase with S, as shown in Figure 2.

As the redshift decreases, the linearly extrapolated critical overdensity $\delta_c(z)$ decreases and both barriers move downward. For a given set of parameters, as the redshift decreases, n_γ increases and $\bar{\rho}_m$ decreases, so that $N_{\rm back}/M$ increases. As a result, the island barrier decreases faster than the bubble barrier for the same decrease in redshift. We cut all the curves in Figure 2 at $\xi\, M_{\rm min}$, which is the scale for which a halo of $M_{\rm min}$ can ionize and set this value as the lower limit of a bubble. In this toy model, we also cut the island scale at $\xi\, M_{\rm min}$, because at smaller scales, the non-linear effect becomes important and the collapse fraction computed from the extended Press–Schechter model (Equation (5)), which is valid for a Gaussian density field, is not accurate anymore. The exact value of the cutoff mass is not critical for the illustrative purpose here. Note that this mass cut of islands is not necessary for the more realistic island model presented in Section 5, in which the lower limit of an island scale is naturally set by the survival limit of islands in the presence of an ionizing background (see the text in Section 5). Below this scale, neutral hydrogen exists only in minihalos or galaxies.

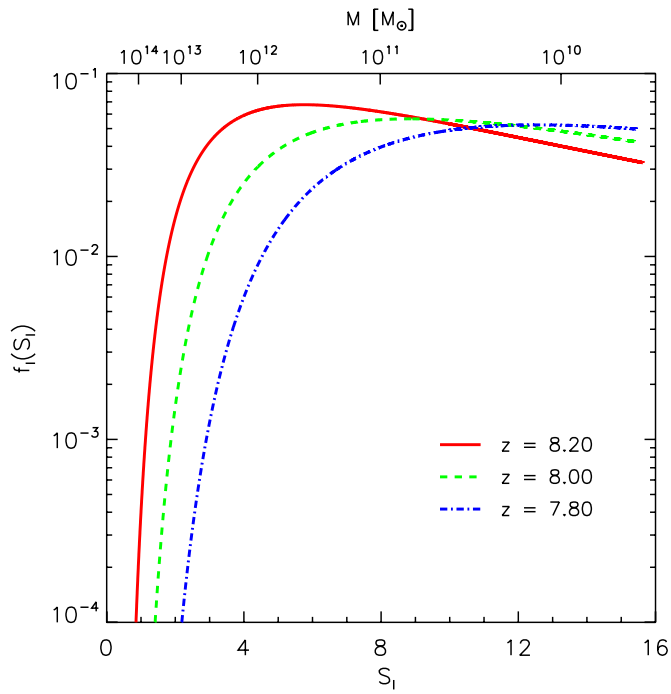

Figure 3. First down-crossing distribution in the island-permeating photon model as a function of the island scale at redshifts 8.2, 8.0, and 7.8, from top to bottom, respectively.

(A color version of this figure is available in the online journal.)

The first down-crossing distribution for the islands in the island-permeating photons model is plotted for three redshifts in Figure 3; S and the corresponding mass scale M are shown on the bottom and top axes, respectively. As expected, at small S, the down-crossing probability is vanishingly small because in this region the barrier is very negative and the average displacement of the random trajectories is still very small. As S increases, the trajectories excurse with wider ranges and in this model the barriers also increase with increasing S, so the crossing probability increases rapidly. For $z = 8.2$, the probability peaks at $S_{\rm I} \approx 5.8$ with $f_{\rm I} \approx 0.07$, then begins to decrease, because for many trajectories the first crossing happened earlier. As the redshift decreases, the island barrier moves downward rapidly and it becomes harder and harder to down-cross it at large scales, with most of the first down-crossings happening at smaller scales. As a result, the first down-crossing probability decreases very rapidly at large scales and it increases at small scales.

The mass functions of islands at three redshifts are plotted in the left panel of Figure 4. The volume filling factors of the neutral islands are $Q_{\rm V}^{\rm I} = 0.70$ ($z = 8.2$), 0.59 ($z = 8.0$), and 0.46 ($z = 7.8$), respectively, and the corresponding ionizing background can be expressed as an H I photoionization rate of $\Gamma_{\rm H\,I} = n_\gamma (1+z)^3\, c\, \sigma_i \approx 1.6 \times 10^{-11}\,{\rm s}^{-1}$. Here, σ_i is the frequency-averaged photoionization cross section of hydrogen. This level of the ionizing background is unreasonably high, because in this toy model we have neglected the effects of dense clumps, minihalos, and any other possible absorbing systems that could limit the mean free path of the ionizing photons.

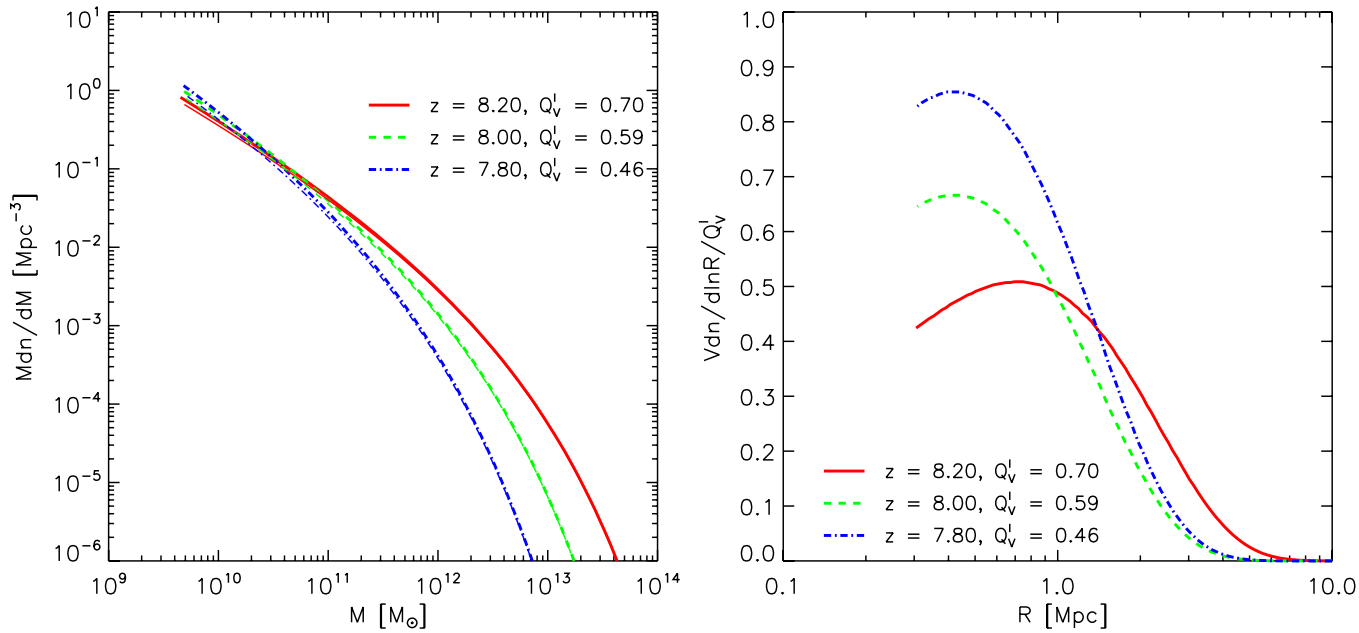

Figure 4. Left panel: the number distribution functions of neutral islands in the model with a uniform island-permeating ionizing background. The numerical solutions are shown as thick curves for redshifts 8.2, 8.0, and 7.8, from top to bottom on the right, respectively. The corresponding volume filling factors of the islands are $Q_V^I = 0.70$ ($z = 8.2$), 0.59 ($z = 8.0$), and 0.46 ($z = 7.8$), respectively. The thin curves show the distribution function given by the analytical form in the linear approximation. Right panel: the size distributions of islands at the same redshifts as in the left panel, normalized by the total neutral fraction Q_V^I.
(A color version of this figure is available in the online journal.)

To facilitate comparisons with the bubble distribution function in Furlanetto et al. (2004), we also plot in the right panel the volume-weighted distribution of the effective radii of the islands computed assuming that the islands are uniform spheres, normalized by the total neutral fraction as in the bubble model. Note that

$$V\frac{dn}{d\ln R} \propto 3M^2\frac{dn}{dM} \propto M\frac{dn}{d\ln M}, \tag{23}$$

so this also reflects how masses are distributed in islands of different sizes.

Unsurprisingly, within a given volume, small islands are much more numerous than larger ones, as shown in the left panel. Similar to the general shape of the volume-weighted bubble size distribution in the bubble model, there is a peak in the island size distribution at each redshift in this model. This means that in the photon-permeating model, the neutral mass is dominated by those islands with a characteristic scale where the distribution peak is located. As redshift decreases, the left panel of Figure 4 shows that the number of large islands decreases rapidly, while the number of the smallest ones even increases a little. This evolutionary behavior is also shown in the right panel of Figure 4, in which large bubbles gradually disappeared, resulting in an increasing curve on the small R end.

In fact, for this toy model, the barrier shape is very close to a straight line, for which a simple analytical solution exists and is very accurate. If we expand the barrier as a linear function of S, we have

$$\delta_I(M, z) = \delta_{I,0} + \delta_{I,1}\, S, \tag{24}$$

where the intercept is

$$\delta_{I,0} \equiv \delta_c(z) - \sqrt{2\,S_{\max}}\,\mathrm{erfc}^{-1}[K(z)] \tag{25}$$

and the slope is

$$\delta_{I,1} \equiv \frac{\mathrm{erfc}^{-1}[K(z)]}{\sqrt{2\,S_{\max}}}. \tag{26}$$

Then, the mass function of the host islands can be expressed analytically:

$$M_I\frac{dn}{dM_I} = \frac{1}{\sqrt{2\pi}}\,\bar{\rho}_{m,0}\left|\frac{dS}{dM_I}\right|\frac{|\delta_{I,0}|}{S^{3/2}(M_I)}\exp\left[-\frac{\delta_I^2(M_I, z)}{2\,S(M_I)}\right]. \tag{27}$$

These are plotted as thin lines in the left panel of Figure 4; we see they almost coincide with the results of numerical solutions (thick lines).

The model of this subsection is only for demonstrating the formalism of calculation with additional (background) ionizing photons and, for simplicity, we assumed that the consumed photons are proportional to the island volume. This is not realistic, because the ionization caused by a background is more likely proportional to the surface area Σ of the island. In the next sections, we shall consider more realistic models.

3.3. The Bubbles-in-islands

Before moving on to more realistic models, let us address the problem of "bubbles-in-island" first. Above, we have assumed that the neutral islands are simple spherical regions, but in fact there might also be self-ionized regions inside an island. This "bubbles-in-island" problem is similar but in the opposite sense of the "voids-in-cloud" problem in the void model (Sheth & van de Weygaert 2004; Paranjape et al. 2012a).

We identify the bubbles inside neutral islands in the excursion set framework by considering the trajectories that first down-crossed the island barrier δ_I at S_I, then at a larger S_B up-crossed over the bubble barrier δ_B. The bubble barrier is the barrier defined without considering the ionizing background, since this

background should be absent inside large neutral regions. Note that in the toy model discussed above, the ionizing background permeates through the neutral islands. It does not make sense to distinguish the island barriers outside and the bubble barriers inside and the problem of bubbles-in-island cannot be discussed.

In the following, we denote the host island scale (including the bubbles inside) and the bubble scale by $S_{\rm I}$ and $S_{\rm B}$, respectively, the first down-crossing distribution by $f_{\rm I}(S_{\rm I}, \delta_{\rm I})$, and the conditional probability for a bubble form inside as $f_{\rm B}(S_{\rm B}, \delta_{\rm B}|S_{\rm I}, \delta_{\rm I})$. The probability distribution of finding a bubble of size $S_{\rm B}$ in a host island of size $S_{\rm I}$ is then given by

$$\mathcal{F}(S_{\rm B}, S_{\rm I}) = f_{\rm I}(S_{\rm I}, \delta_{\rm I}) \cdot f_{\rm B}(S_{\rm B}, \delta_{\rm B}|S_{\rm I}, \delta_{\rm I}). \quad (28)$$

The neutral mass of an island is given by the total mass of the host island minus the masses of bubbles of various sizes embedded in the host island, i.e.,

$$M = M_{\rm I}(S_{\rm I}) - \sum_i M_{\rm B}^i\left(S_{\rm B}^i\right). \quad (29)$$

The conditional probability distribution $f_{\rm B}(S_{\rm B}, \delta_{\rm B}|S_{\rm I}, \delta_{\rm I})$ characterizes the size distribution of bubbles inside an island of scale $S_{\rm I}$ and overdensity $\delta_{\rm I}$ and $f_{\rm B}(S_{\rm B}, \delta_{\rm B}|S_{\rm I}, \delta_{\rm I})dS_{\rm B}$ is the conditional probability of a random walk that first up-crosses $\delta_{\rm B}$ between $S_{\rm B}$ and $S_{\rm B} + dS_{\rm B}$, given a starting point of $(S_{\rm I}, \delta_{\rm I})$.

In order to compute $f_{\rm B}$, we could effectively shift the origin point of coordinates to the point $(S_{\rm I}, \delta_{\rm I})$, then the method developed by Zhang & Hui (2006) is still applicable. The effective bubble barrier becomes:

$$\delta_{\rm B}' = \delta_{\rm B}(S + S_{\rm I}) - \delta_{\rm I}(S_{\rm I}), \quad (30)$$

where $S = S_{\rm B} - S_{\rm I}$. Given an island $(S_{\rm I}, \delta_{\rm I})$, on average, the fraction of volume (or mass) of the island occupied by bubbles of different sizes is

$$q_{\rm B}(S_{\rm I}, \delta_{\rm I}; z) = \int_{S_{\rm I}}^{S_{\rm max}(\xi \cdot M_{\rm min})} [1 + \delta_{\rm I}\, D(z)] f_{\rm B}(S_{\rm B}, \delta_{\rm B}|S_{\rm I}, \delta_{\rm I}) dS_{\rm B}. \quad (31)$$

The factor $[1 + \delta_{\rm I}\, D(z)]$ enters because these bubbles are in the environment with underdensity of $\delta_{\rm I}\, D(z)$, where $D(z)$ is the linear growth factor. Then, the net neutral mass of the host island can be written as $M = M_{\rm I}(S_{\rm I})\,[1 - q_{\rm B}(S_{\rm I}, \delta_{\rm I}; z)]$. Taking into account the effect of bubbles-in-island, the neutral mass function of the islands at a redshift z is

$$\frac{dn}{dM}(M, z) = \frac{dn}{dM_{\rm I}}\frac{dM_{\rm I}}{dM} = \frac{\bar{\rho}_{\rm m,0}}{M_{\rm I}} f_{\rm I}(S_{\rm I}, z)\left|\frac{dS_{\rm I}}{dM_{\rm I}}\right|\frac{dM_{\rm I}}{dM}. \quad (32)$$

4. THE IONIZING BACKGROUND

The intensity of the ionizing background is very important in the late reionization epoch. However, it has only been constrained after reionization from the mean transmitted flux in the Lyman-α forest (e.g., Wyithe & Bolton 2011; Calverley et al. 2011) and in any case it evolves with redshift and depends on the detailed history of reionization. Conversely, the evolution of the ionizing background also affects the reionization process.

In the toy model presented in Section 3.2, we considered an island-permeating ionizing background, for which the absorptions from dense clumps are neglected and the resulting intensity of the ionizing background is unreasonably high. Here, we give a more realistic model for the ionizing background. Due to the existence of dense clumps that have high recombination rates and limit the mean free path of the ionizing background photons, an island does not see all the ionizing photons emitted by all the sources, but only out to a distance of roughly the mean free path of the ionizing photons. The comoving number density of background ionizing photons at a redshift z can be modeled as the integration of escaped ionizing photons that are emitted from newly collapsed objects that survived to the distances between the sources and the position under consideration:

$$n_\gamma(z) = \int_z \bar{n}_{\rm H}\left|\frac{df_{\rm coll}(z')}{dz'}\right| f_\star\, N_{\gamma/{\rm H}}\, f_{\rm esc}\, \exp\left[-\frac{l(z, z')}{\lambda_{\rm mfp}(z)}\right] dz', \quad (33)$$

where $l(z, z')$ is the physical distance between the source at redshift z' and the redshift z under consideration and $\lambda_{\rm mfp}$ is the physical mean free path of the background ionizing photons.

Various absorption systems could limit the mean free path of the background ionizing photons. The most frequently discussed absorbers are LLSs, which have large enough H I column densities to remain self-shielded (e.g., Miralda-Escudé et al. 2000; Furlanetto & Oh 2005; Bolton & Haehnelt 2013). Minihalos are also self-shielding systems that could block ionizing photons. Furlanetto & Oh (2005) developed a simple model for the mean free path of ionizing photons in a universe where minihalos dominate the recombination rate. However, as also discussed in Furlanetto & Oh (2005), the formation and the abundance of minihalos are highly uncertain (Oh & Haiman 2003) and minihalos would be probably evaporated during the late epoch of reionization (Barkana & Loeb 1999; Shapiro et al. 2004), although they may consume substantial ionizing photons before they are totally evaporated (Iliev et al. 2005). In addition to LLSs and minihalos, the accumulative absorption by low column density systems cannot be neglected (Furlanetto & Oh 2005), but the quantitative contributions from these systems are quite uncertain and need to be calibrated by high-resolution simulations or observations.

Here, we focus on the effect of LLSs on the mean free path of ionizing photons and use a simple model for the IGM density distribution developed by Miralda-Escudé et al. (2000, hereafter MHR00). In the MHR00 model, the volume-weighted density distribution of the IGM measured from numerical simulations can be fit by the formula

$$P_{\rm V}(\Delta)\, d\Delta = A_0\, \exp\left[-\frac{(\Delta^{-2/3} - C_0)^2}{2\,(2\delta_0/3)^2}\right]\Delta^{-\beta}\, d\Delta \quad (34)$$

for $z \sim 2$–6, where $\Delta = \rho/\bar{\rho}$. Here, δ_0 and β are parameters fitted to simulations. The value of δ_0 can be extrapolated to higher redshifts by the function $\delta_0 = 7.61/(1 + z)$ (MHR00) and we take $\beta = 2.5$ for the redshifts of interest. The parameters A_0 and C_0 are set by normalizing $P_{\rm V}(\Delta)$ and $\Delta P_{\rm V}(\Delta)$ to unity.

Using the density distribution of the IGM, the mean free path of ionizing photons can be determined by the mean distance between self-shielding systems with relative densities above a critical value $\Delta_{\rm crit}$ and can be written as (Choudhury & Ferrara 2005, MHR00)

$$\lambda_{\rm mfp} = \frac{\lambda_0}{[1 - F_{\rm V}(\Delta_{\rm crit})]^{2/3}}, \quad (35)$$

where $F_V(\Delta_{crit})$ is the volume fraction of the IGM occupied by regions with the relative density lower than Δ_{crit}, given by

$$F_V(\Delta_{crit}) = \int_0^{\Delta_{crit}} P_V(\Delta)\, d\Delta. \tag{36}$$

Following Schaye (2001) and assuming photoionization equilibrium and a Case A recombination rate, the critical relative density for a clump to self-shield can be approximately written as (see also Furlanetto & Oh 2005; Bolton & Haehnelt 2013, MHR00)

$$\Delta_{crit} = 36\, \Gamma_{-12}^{2/3}\, T_4^{2/15} \left(\frac{\mu}{0.61}\right)^{1/3} \left(\frac{f_e}{1.08}\right)^{-2/3} \left(\frac{1+z}{8}\right)^{-3}, \tag{37}$$

where $\Gamma_{-12} = \Gamma_{\rm H\,I}/10^{-12}\,{\rm s}^{-1}$ is the hydrogen photoionization rate in units of $10^{-12}\,{\rm s}^{-1}$, $T_4 = T/10^4\,{\rm K}$ is the gas temperature in units of $10^4\,{\rm K}$, μ is the mean molecular weight, and $f_e = n_e/n_{\rm H}$ is the free electron fraction with respect to hydrogen. For the mostly ionized IGM during the late stage of reionization, we assume $T_4 = 2$.

The H I photoionization rate $\Gamma_{\rm H\,I}$ in Equation (37) is related to the total number density of ionizing photons n_γ in Equation (33) by

$$\Gamma_{\rm H\,I} = \int \frac{dn_\gamma}{d\nu}\, (1+z)^3\, c\, \sigma_\nu\, d\nu, \tag{38}$$

where $dn_\gamma/d\nu$ is the spectral distribution of the background ionizing photons, c is the speed of light, and $\sigma_\nu = \sigma_0\,(\nu/\nu_0)^{-3}$ with $\sigma_0 = 6.3 \times 10^{-18}\,{\rm cm}^2$ and ν_0 being the frequency of hydrogen ionization threshold. Assuming a power-law spectral distribution of the form $dn_\gamma/d\nu = (n_\gamma^0/\nu_0)(\nu/\nu_0)^{-\eta-1}$, in which n_γ^0 is related to the total photon number density n_γ by $n_\gamma = n_\gamma^0/\eta$, then the H I photoionization rate can be written as

$$\Gamma_{\rm H\,I} = \frac{\eta}{\eta+3}\, n_\gamma\, (1+z)^3\, c\, \sigma_0. \tag{39}$$

In the following, we assume $\eta = 3/2$ to approximate the spectra of starburst galaxies (Furlanetto & Oh 2005).

It has been suggested that the characteristic length λ_0 in Equation (35) is related to the Jeans length and can be fixed by comparing with low-redshift observations (Choudhury & Ferrara 2005; Kulkarni et al. 2013). We take $\lambda_0 = A_{\rm mfp} r_{\rm J}$, where $r_{\rm J}$ is the physical Jeans length. Taking the proportional constant $A_{\rm mfp}$ as a free parameter, the comoving number density of background ionizing photons n_γ or, equivalently, the H I photoionization rate $\Gamma_{\rm H\,I}$, can be solved by combining Equations (33)–(37) and (39). We scale the hydrogen photoionization rate to be $\Gamma_{\rm H\,I} = 10^{-12.8}\,{\rm s}^{-1}$ at redshift 6, as suggested by recent measurements from the Lyman-α forest (Wyithe & Bolton 2011; Calverley et al. 2011). Then, the parameter $A_{\rm mfp}$ is constrained to be $A_{\rm mfp} = 0.482$. The redshift evolution of the hydrogen photoionization rate due to the ionizing background is shown in Figure 5. Note that by scaling the background photoionization rate of hydrogen to the observed value, we implicitly take into account the possible absorptions due to minihalos and low column density systems.

In the above treatment of the ionizing background, the derived intensity is effectively the value averaged over the whole universe. Due to the clustering of the ionizing sources, however, the ionizing background should fluctuate significantly from place to place at the end of reionization. The detailed space fluctuations of the ionizing background would be challenging to incorporate and for the purpose of illustrating the island model and predicting the statistical results in the next section, we use here a uniform ionizing background with the averaged intensity.

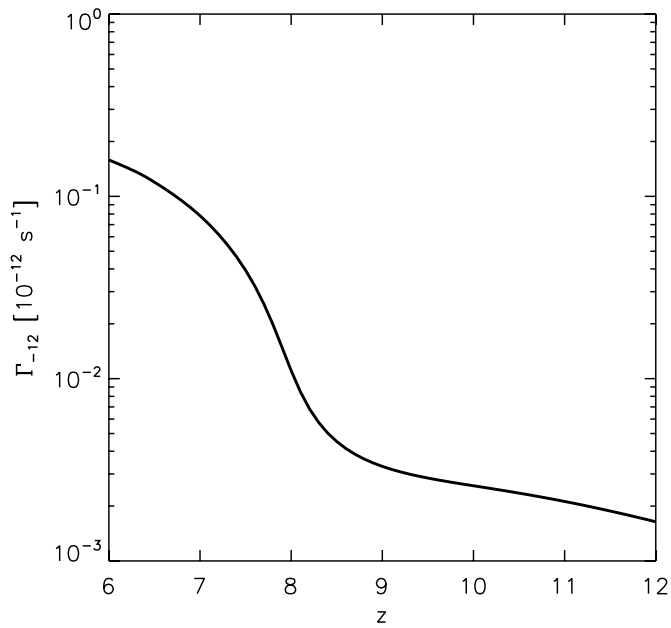

Figure 5. Redshift evolution of the hydrogen ionization rate Γ_{-12}.

5. THE ISLAND MODEL OF REIONIZATION

5.1. Ionization at the Surfaces of Neutral Islands

We now use the excursion set model developed above to study the neutral islands during the reionization process. In Section 3.2, we used a simple toy model to illustrate the basic formalism, but we have noted that it is based on an unrealistic assumption that the ionizing photons permeate through the neutral islands. Here, we consider more physically motivated model assumptions.

We assume that a spatially homogeneous ionizing background flux is established throughout all of the ionized regions at redshift $z_{\rm back}$. These ionizing photons cannot penetrate the neutral islands, but were consumed near the surface of the islands. We may then assume that the number of photons consumed by an island at any instant is proportional to its surface area or, in terms of mass, $M^{2/3}$. The number of background ionizing photons consumed is then given by

$$N_{\rm back} = \int F(z)\, \Sigma_{\rm I}(t)\, dt, \tag{40}$$

where $\Sigma_{\rm I}$ is the physical surface area of the neutral island, while $F(z)$ is the physical number flux of background ionizing photons, which is related to the comoving photon number density by $F(z) = n_\gamma(z)\,(1+z)^3\, c/4$. For spherical islands, the surface area is related to the scale radius by $\Sigma_{\rm I} = 4\pi R^2/(1+z)^2$, in which R is in comoving coordinates. For non-spherical islands, one could still introduce a characteristic scale R and the area would be related to R^2. In fact, under the action of the ionizing background, non-spherical neutral regions have a tendency to evolve to spherical ones because a sphere has a minimum surface area for a given volume.

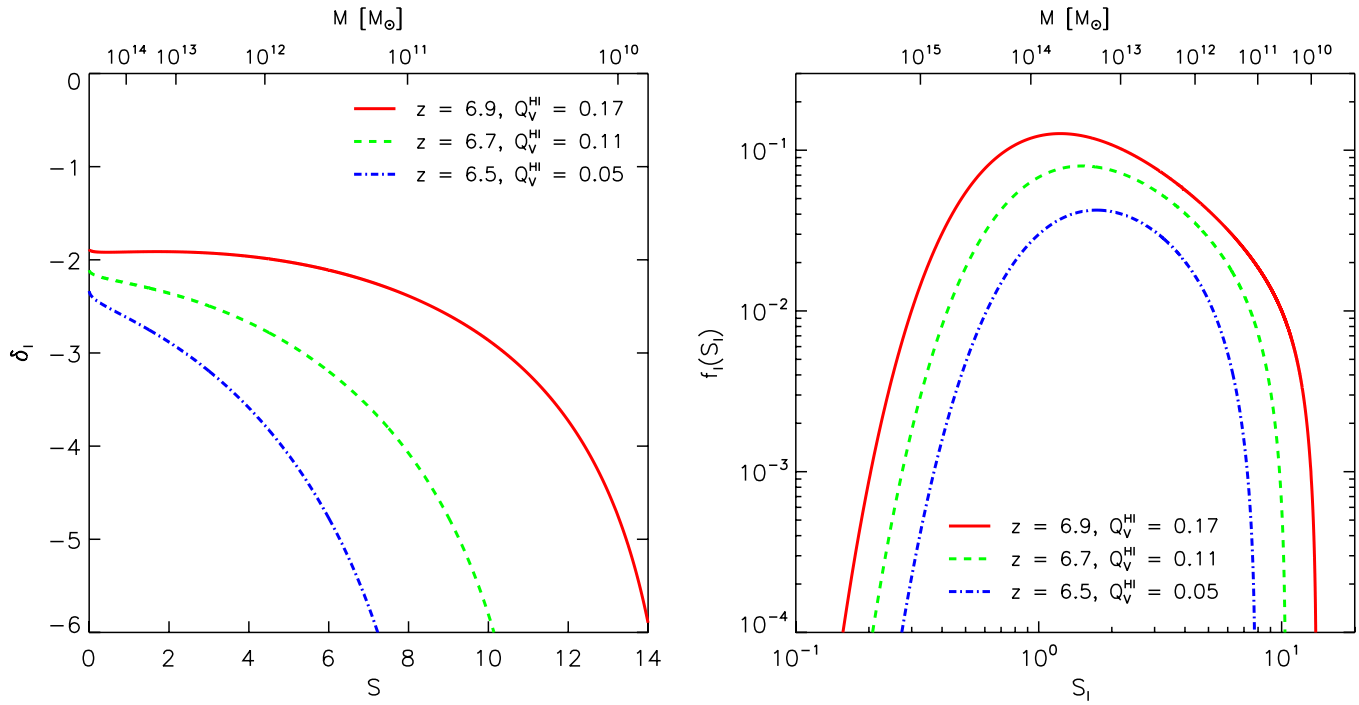

Figure 6. Left panel: the island barriers for our fiducial model. The solid, dashed, and dot-dashed curves are for redshifts 6.9, 6.7, and 6.5, from top to bottom, respectively, and the corresponding neutral fractions of the universe (excluding the bubbles-in-islands) are $Q_V^{HI} = 0.17$, 0.11, and 0.05, respectively. Right panel: the corresponding first down-crossing distributions at the same redshifts as in the left panel.

(A color version of this figure is available in the online journal.)

The usual excursion set approach does not contain time or history and everything is determined from the information at a given redshift. However, we see from Equation (40) that the consumption of the ionizing background photons by an island depends on its history. Below, we try to solve this problem by considering some simplified assumptions. We assume that the neutral islands shrink with time and the hydrogen number density around an island is nearly a constant, which is approximately true when we are considering large scales. For simplicity, let us consider a spherical island. When the island shrinks, counting the required number of ionizations gives

$$n_{\rm H}(R)(1+\bar{n}_{\rm rec})\,4\pi R^2\,(-dR) = F(z)\,\frac{4\pi R^2}{(1+z)^2}\,dt, \qquad (41)$$

where the hydrogen number density $n_{\rm H}$ is in comoving coordinates, so that

$$\frac{dR}{dt} = -\frac{F(z)/(1+z)^2}{n_{\rm H}(R)(1+\bar{n}_{\rm rec})} \approx -\frac{F(z)/(1+z)^2}{\bar{n}_{\rm H}(1+\bar{n}_{\rm rec})}. \qquad (42)$$

Integrating from the background onset redshift $z_{\rm back}$ to redshift z, we have

$$\Delta R \equiv R_i - R_f = \int_z^{z_{\rm back}} \frac{F(z)}{\bar{n}_{\rm H}(1+\bar{n}_{\rm rec})}\,\frac{dz}{H(z)(1+z)^3}, \qquad (43)$$

where R_i and R_f denote the initial and final scale of the island, respectively. This shows that the change in R is independent of the mass of the island, but depends solely on the elapsed time. The total number of background ionizing photons consumed is given by

$$N_{\rm back} = \frac{4\pi}{3}\left(R_i^3 - R_f^3\right)\bar{n}_{\rm H}(1+\bar{n}_{\rm rec}). \qquad (44)$$

5.2. Island Size Distribution

With this model for the consumption behavior of the background ionizing photons, and taking the fiducial set of parameters, we plot the island barriers of in Equation (12) in the left panel of Figure 6 for several redshifts. The corresponding first down-crossing distributions as a function of the host island scale $S_{\rm I}$ (i.e., including ionizing bubbles inside the island) are plotted in the right panel of Figure 6.

Unlike the toy model with permeating ionizing photons, in this model the shape of the island barriers is drastically different from the bubble barriers; hence, the different shape of the first down-crossing distribution curves. The island and bubble barriers have the same intercept at $S \sim 0$, because on very large scales, the contribution of the ionizing background, which is proportional to the surface area, would become unimportant when compared with the contribution of the self-ionization, which is proportional to the volume. However, the island barriers bend downward at $S > 0$ because of the contribution of the ionizing background. As the barrier curves become gradually steeper when approaching larger S, it is increasingly harder for the random walks to first down-cross them at smaller scales, even though on the smaller scales the dispersion of the random trajectory grow larger. As a result, the first down-crossing distribution rapidly increases to a peak value and drops down on small scales and there is a mass cut on the host island scale, $M_{\rm I,min}$, at each redshift in order to make sure $K(M,z) \geqslant 0$. This lower cut on the island mass scale assures $\Delta R \leqslant R_i$, i.e., the whole island is not completely ionized during this time by the ionizing background and $M_{\rm I,min}$ is the minimum mass of the host island at $z_{\rm back}$ that can survive until a redshift z under consideration.

The mass distribution function of the host islands can be obtained directly from Equation (19), from which we can see

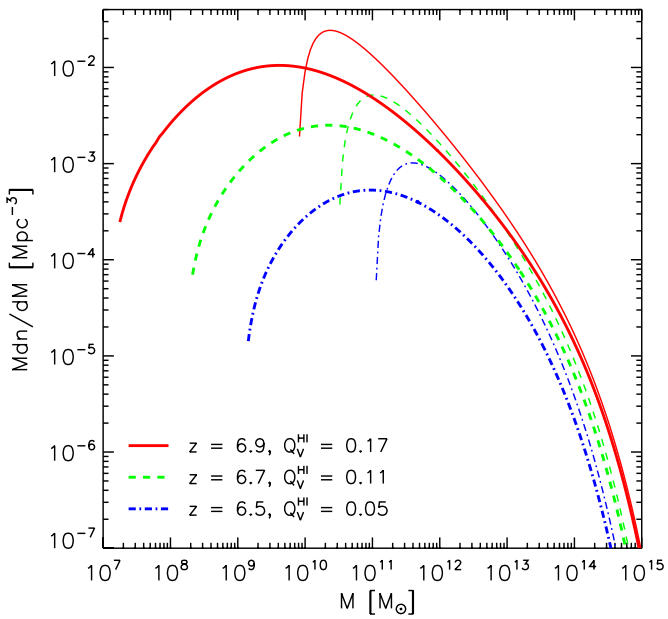

Figure 7. Mass function of the host islands in terms of the mass at a redshift z (thick lines) and the initial mass at a redshift $z_{\rm back}$ (thin lines) for our fiducial model. The solid, dashed, and dot-dashed lines are for $z = 6.9$, 6.7, and 6.5, from top to bottom, respectively.

(A color version of this figure is available in the online journal.)

clearly the shrinking process of these islands. What we are interested is the mass of the host island at redshift z, but the mass scale M in Equations (11)–(13) is the initial island mass at redshift $z_{\rm back}$. We may convert the two masses using Equation (43):

$$\frac{M_f}{M_i} = \left(1 - \frac{\Delta R}{R_i}\right)^3. \tag{45}$$

Islands with an initial radius $R_i < \Delta R$ would not survive and islands with a larger radius would also evolve into smaller ones.

The distributions of the host island mass (including ionized bubbles inside) are plotted for $z = 6.9$, 6.7, and 6.5 in Figure 7 as thick lines. The distributions of the corresponding progenitors at redshift $z_{\rm back}$ are plotted as thin lines. Using our fiducial model parameters, the volume filling factors of these progenitors at $z_{\rm back}$ are $Q_{\rm V,i}^{\rm host} = 0.51$, 0.31, and 0.14, for the host islands that survive at $z = 6.9$, 6.7, and 6.5, respectively. The initial mass distribution of these progenitors all have a very steep lower mass cutoff, because below that minimal mass by redshift z the whole island would be completely ionized by the background photons. Due to the mapping of Equation (45), the cutoff in the final mass distribution is not as sharp as the initial mass distribution and the whole distribution curve begins to bend down at lower masses.

5.3. Bubbles-in-islands

However, the total mass function of the host islands does not give a full picture of the reionization process, since there could be ionized bubbles inside these islands. Even though the outside ionization background is shielded from the center of the neutral islands, there might be galaxies that form inside the neutral islands and the photons emitted by these galaxies ionize part of the islands. The neutral islands are located in underdense regions, so fewer galaxies formed. Nevertheless, by the end of the epoch of reionization, galaxy formation inside them cannot be neglected.

As discussed in Section 3.3, the distribution of bubbles in an island can be calculated from the conditional probability of up-crossing the bubble barrier after down-crossing the island barrier. We plot the resulting mass function of inside bubbles for three different host islands at redshift $z = 6.9$ in the left panel of Figure 8. The masses of the host islands are

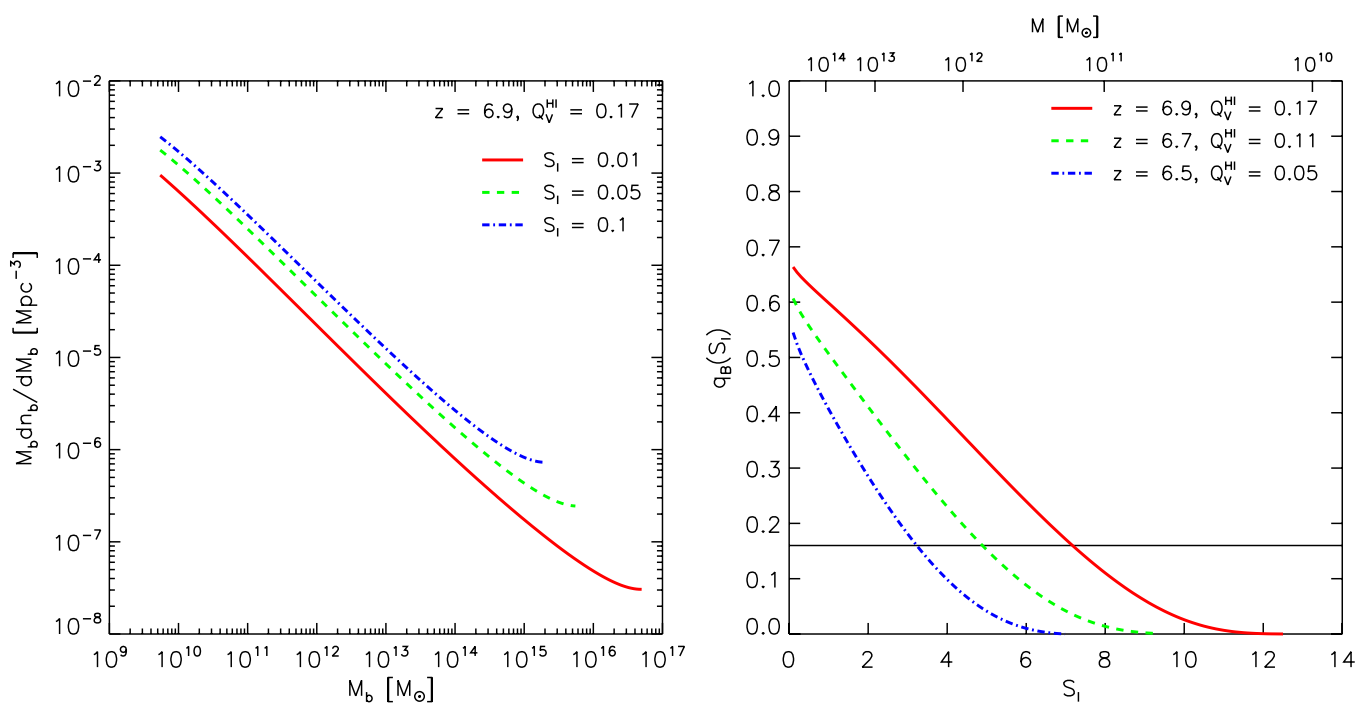

Figure 8. Left panel: the mass function of bubbles in an island of scale $S_{\rm I} = 0.01$, 0.05, and 0.1, from bottom to top, respectively. The redshift shown here is 6.9. Right panel: the average mass fraction of bubbles in an island as a function of the island scale at redshifts $z = 6.9$, 6.7, and 6.5, from top to bottom, respectively. The percolation threshold $p_c = 0.16$ is also shown as the horizontal line.

(A color version of this figure is available in the online journal.)

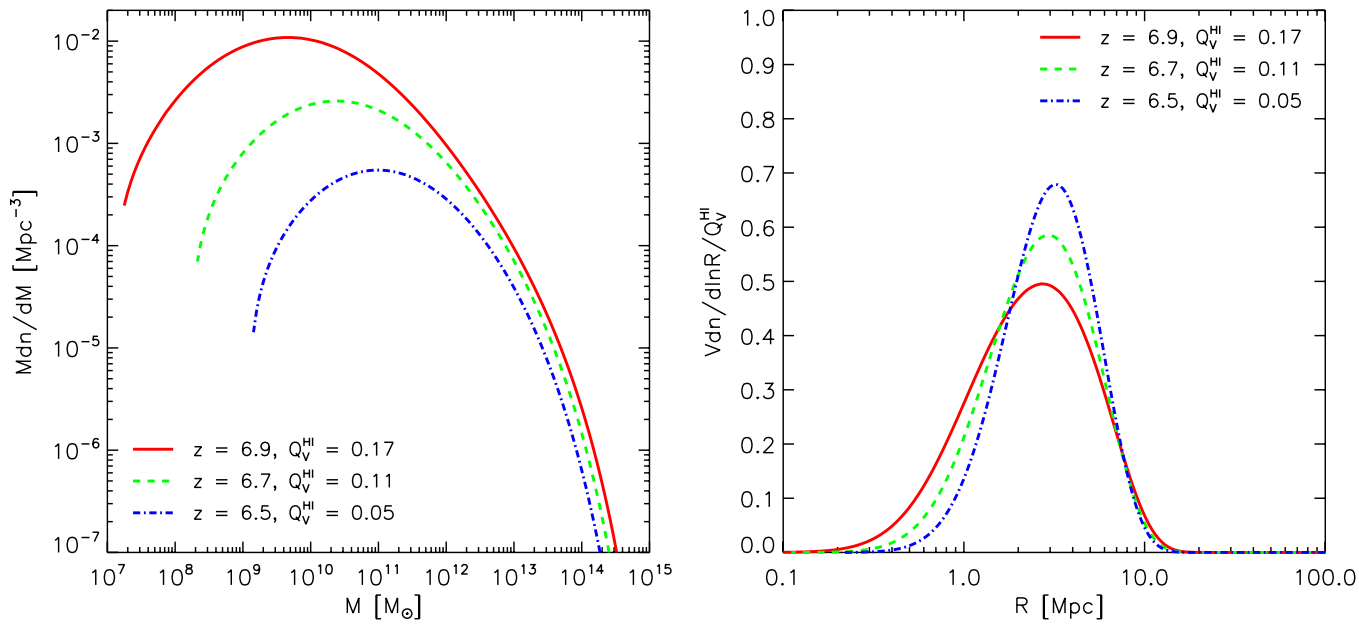

Figure 9. Left panel: the mass function of neutral islands at redshift $z = 6.9$, 6.7, and 6.5, from top to bottom, respectively. The corresponding volume filling factor of the neutral islands at these redshifts are $Q_V^{H\,I} = 0.17$, 0.11, and 0.05, respectively. Right panel: the size distribution of neutral islands, with the scale R converted from their volume, at redshifts $z = 6.9$, 6.7, and 6.5, from bottom to top at the center, respectively.

(A color version of this figure is available in the online journal.)

$M \approx 2 \times 10^{17} M_\odot$ ($S_I = 0.01$), $2 \times 10^{16} M_\odot$ ($S_I = 0.05$), and $8 \times 10^{15} M_\odot$ ($S_I = 0.1$), from bottom to top, respectively. We see the bubbles-in-islands follow a power-law distribution, with small bubbles being more numerous. The upward trend at the large-scale end on each mass distribution curve is due to the numerical error in the up-crossing probability when the inside bubble scale approaches the host island scale.

To assess the total amount of bubbles-in-islands, we plot in the right panel of Figure 8 the average mass fraction of bubbles-in-island as a function of the host island mass. We see that there could be a sizable fraction of the host island that is ionized from within, especially for the larger islands. At $z = 6.9$ and for $M > 10^{12} M_\odot$, this fraction is higher than 35% and it is higher than 60% for $M > 10^{14} M_\odot$ host islands at the same redshift, so within these large neutral islands smaller ionized bubbles flourish. From the excursion set point of view, it is not unusual for the random trajectory to increase the bubble barrier after just down-crossing the island barrier, especially at large scales where the displacement between the island barrier and the bubble barrier is small. Therefore, even though the whole region is underdense, a large fraction of it could be sufficiently dense for galaxies to form and create ionized regions around them. The bubble fraction drops sharply for smaller islands, because the island barrier departs from the bubble barrier rapidly at small scales and it is less likely to form galaxies inside small islands with very low densities. Interestingly, as redshift decreases, this fraction decreases. For $z = 6.5$, it is about 7% for $M \sim 10^{12} M_\odot$ host islands and about 42% for $M \sim 10^{14} M_\odot$ host islands. This is because what are left at later times are relatively deep underdense regions and the probability of forming galaxies in such underdense environments is lower.

Excluding the bubbles-in-islands, we plot the mass function and the size distribution of the net neutral islands in the left and right panels of Figure 9, respectively. The solid, dashed, and dot-dashed lines are for $z = 6.9$, 6.7, and 6.5, with a volume filling factor of the net neutral islands of $Q_V^{H\,I} = 0.17$ ($z = 6.9$), 0.11 ($z = 6.7$), and 0.05 ($z = 6.5$), respectively. Similar to the host island mass function shown in Figure 7, there is also a small-scale cutoff on the neutral island mass due to the existence of an ionizing background. Because of the high bubbles-in-island fraction in large host islands, excluding the bubbles-in-islands results in much fewer large islands. As seen from the size distribution in the right panel, in which the scale R is converted from the neutral island volume assuming a spherical shape, both the mass fractions of large and small islands decrease with time and the distribution curve becomes sharper and sharper, but the characteristic scale of the neutral islands remains almost unchanged.

Figure 9 shows basically the number and mass distribution of the neutral components of the host islands. However, the results of the bubbles-in-island fraction in the right panel of Figure 8 show that within large host islands, a large fraction of the island volume could be ionized by the photons from newly formed galaxies within. A naive application of the host island mass function may greatly overestimate the mean neutral fraction of the universe, while the application of the neutral island size distribution, as shown in the right panel of Figure 9, would never reveal the real image of the ionization field. Indeed, if there are so many ionized bubbles inside large neutral islands, it may be difficult to visually identify the host islands. In light of this, we need to consider the condition under which the isolated island picture is still applicable. In particular, if the bubbles inside an island are so numerous and large as to overlap with each other, they may form a network that percolates through the whole island, thereby breaking the island into pieces or forming a sponge-like topology of neutral and ionized regions.

5.4. Percolation Model

Within the spherical model, it is difficult to deal with the sponge-like topology, but we may limit ourselves to the case where the treatment is still valid. According to the theory of percolation, in a binary phase system, percolation of one phase occurs when the filling factor of it exceeds a threshold fraction p_c (see, e.g., Bunde & Havlin 1991). In the context of

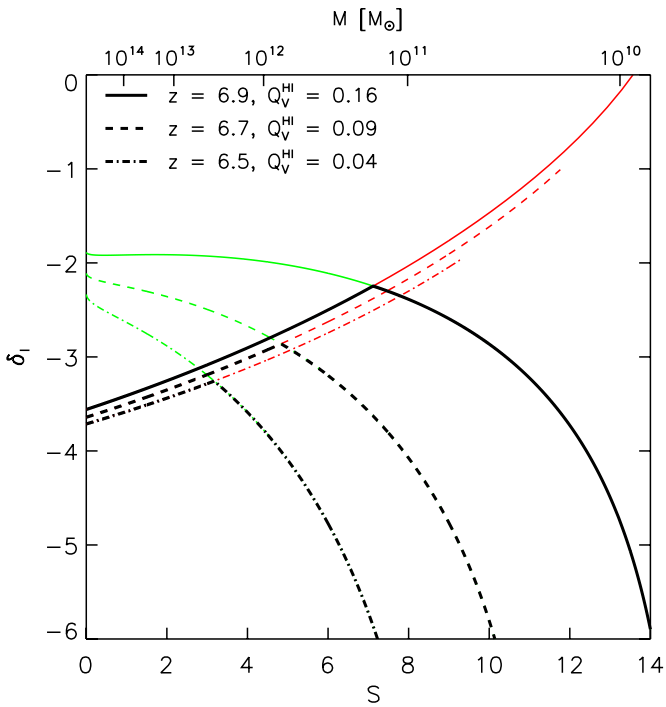

Figure 10. Basic island barriers (green curves), the percolation threshold induced barriers (red curves), and the effective island barriers (black curves) for our fiducial model. The solid, dashed, and dot-dashed curves are for redshifts 6.9, 6.7, and 6.5, from top to bottom, respectively.

(A color version of this figure is available in the online journal.)

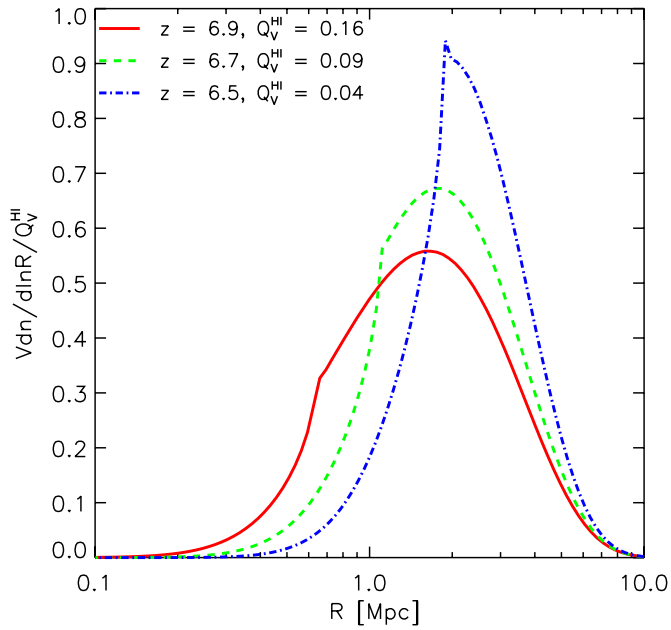

Figure 11. Size distribution of neutral islands in our fiducial model taking into account the bubbles-in-island effect and the p_c cutoff on the bubbles-in-island fraction. The solid, dashed, and dot-dashed curves are for redshifts $z = 6.9$, 6.7, and 6.5, respectively, and the corresponding volume filling factors of neutral islands are $Q_V^{HI} = 0.16$ ($z = 6.9$), 0.09 ($z = 6.7$), and 0.04 ($z = 6.5$), respectively.

(A color version of this figure is available in the online journal.)

cosmology, Klypin & Shandarin (1993) obtained the percolation threshold p_c for the clustered large-scale structures from cosmological simulations. However, the spatial distribution of ionized bubbles and neutral islands is much less filamentary than the gravitationally clustered dark matter or galaxies. As the ionization field follows the density field (Battaglia et al. 2012b), which is almost Gaussian on large scales (Planck Collaboration et al. 2013b), here we use the percolation threshold for a Gaussian random field of $p_c = 0.16$ (Klypin & Shandarin 1993), below which we may assume that the bubbles-in-island do not percolate through the whole island.

The problem of percolation appears in several stages of reionization. At the early stage of reionization, the filling factor of ionized bubbles increases as the bubble model predicted. Once the bubble filling factor becomes larger than the percolation threshold p_c, the ionized bubbles are no longer isolated and the predictions made from the bubble model are not accurate anymore. Therefore, the threshold p_c sets a critical redshift z_{Bp}, below which the bubble model may not be reliable. Similarly, the model of neutral islands can make accurate predictions only below a certain redshift z_{Ip}, when the island filling factor is below p_c. The ionizing background was set up after the ionized bubbles percolated but before the islands were all isolated, so $z_{Bp} > z_{back} > z_{Ip}$. Finally, the percolation threshold may also be applied to the bubbles-in-island fraction. An island with a high value of q_B may not qualify as a whole neutral island and the bubbles inside it are probably not isolated regions.

It may be desirable to consider also the distribution of those bona fide neutral islands, for which the bubble fraction is below the percolation threshold, i.e., after excluding those islands with $q_B > p_c$. This percolation criterion of $q_B < p_c$ acts as an additional barrier for finding islands; those islands with high bubbles-in-island fractions are excluded, but the neutral regions in them contribute to the number of smaller islands. This additional barrier is obtained by solving $q_B(S_I, \delta_I; z) < p_c$, and is plotted in Figure 10 with red lines for redshift $z = 6.9$, 6.7, and 6.5, from top to bottom, respectively. The basic island barriers are also plotted in the same figure with green lines. The combined effective island barriers are shown as black lines. The barrier that results from the percolation criterion takes effect at large scales as larger islands could have larger bubbles-in-island fractions and larger-scale islands need to be more underdense to keep the whole region mostly neutral. The basic island barrier (Equation (12)) is effective on small scales, because small islands can be more easily swallowed by the ionizing background. According to the percolation criterion, the island model can be reasonably applied at redshifts below $z_{Ip} \sim 6.9$ in our fiducial model, although for other parameter sets the value would be different.

With the combined island barrier taking into account the bubbles-in-island effect, we find host islands by computing the first down-crossing distribution and find bubbles in them by computing the conditional first up-crossing distribution with respect to the bubble barrier. Subtracting the bubbles-in-islands, the mass distribution of the neutral islands and the volume filling factor of the neutral components Q_V^{HI} are obtained. The resulting size distribution of the neutral islands in terms of the effective radii is plotted in Figure 11 for redshifts $z = 6.9$, 6.7, and 6.5. The distribution curve is normalized by the total neutral fraction in each redshift, which is $Q_V^{HI} = 0.16$ ($z = 6.9$), 0.09 ($z = 6.7$), and 0.04 ($z = 6.5$), respectively.

We note that after applying the p_c cutoff, the resulting neutral fraction at a specific redshift differs a little from the model without the p_c cutoff. Intuitively, the percolation threshold acts only as a different definition of islands and should not change the ionization state of the IGM. This is true because those islands excluded by the percolation threshold will be considered to

be pieces of smaller islands that still contribute to the total neutral fraction. However, two competitive facts are taking effect in our island-finding procedure, which could make the results different. First, we have assumed that the bubbles-in-islands are all ionized, but neglected those small islands that could possibly exist in these relatively large bubbles. When applying the p_c cutoff, some large islands with large bubbles are excluded and the random walk would continue to enter the scales smaller than the bubbles and could possibly find smaller islands that are embedded in large bubbles. Therefore, the model with a p_c cutoff could find more small islands that are not accounted for in the model without a p_c cutoff and it tends to predict higher neutral fraction. On the other hand, one large island with a large bubbles-in-island fraction is taken as several smaller islands in the model with a p_c cutoff and small islands are more significantly influenced by the ionizing background. This fact results in a lower neutral fraction for the model with a p_c cutoff. As the redshift decreases, more and more small islands are swallowed by the ionizing background, so the second effect gradually dominates over the first one. With the fiducial parameters used here, the second effect dominates for the redshifts of interest and the neutral fractions predicted in the model with a p_c cutoff are slightly lower than in the model without a p_c cutoff.

As shown in Figure 11, in this model, the island size distribution after $z_{\rm Ip}$ also has a peak. For this set of model parameters, the characteristic size of neutral islands at $z = 6.9$ is about 1.6 Mpc, but the distribution extends over a range, with the lower value as small as 0.2 Mpc and the high value as large as 10 Mpc. As the redshift decreases, small islands disappear rapidly because of the ionizing background. This is qualitatively consistent with simulation results (Shin et al. 2008) in which small islands are much rarer during late reionization compared with those small ionized bubbles in the early stage. As the reionization proceeds, the large islands shrink and the small islands are swallowed by the ionizing background, with the small ones disappearing more rapidly and the peak position of the distribution curve shifting slightly toward larger scales, but it does not change much. Due to the rapidly decreasing number of small islands, the distribution curve becomes narrower. The distribution also becomes taller with decreasing redshift because it is normalized against the volume neutral fraction $Q_{\rm V}^{\rm H\,I}$ at each redshift. With $Q_{\rm V}^{\rm H\,I}$ decreasing, the normalized distribution has narrower and higher peaks, but the absolute number of neutral islands per comoving volume is decreasing.

6. CONCLUSION

This paper is devoted to the understanding of the late stage of the epoch of reionization. According to the bubble model (Furlanetto et al. 2004) and radiative transfer simulations, reionization started with the ionization of regions with higher-than-average densities, as stars and galaxies formed earlier in such regions, while the regions with lower-than-average densities remained neutral for a longer time. Inspired by the bubble model, here we try to understand the evolution of the remaining large neutral regions during the late stage of reionization, which we call "islands." We developed a model of their mass distribution and evolution based on excursion set theory. The excursion set theory is appropriate for constructing the ionized bubble model and the neutral island model because the reionization field follows the density field on large scales (Battaglia et al. 2012b).

With the inclusion of an ionizing background, which should exist after the percolation of ionized regions, we set an island barrier on the density contrast in the excursion set theory for the islands to remain neutral and an island was identified when the random walk first down-crosses the island barrier. We presented algorithms for computing the first down-crossing distribution, obtained mass function for the islands, and also provide a semi-empirical way to determine the intensity of the ionizing background during the late reionization era.

We first illustrated the formalism of computation with a simple toy model, where the number of consumed ionizing background photons per unit time is proportional to the volume of the island, i.e., the ionizing background is uniformly distributed within the island. While this is not realistic, it is a relatively simple way of deriving the analytical expression of the neutral island mass function. The model predicts a large number of small islands. We then considered a more realistic model, where the ionizing background only causes the ionization at the surface of the island, so that the consumption rate of the ionizing background is proportional to the surface area of the island. Under the action of such ionizing photons, an island would shrink with time. The larger islands shrink, while smaller ones disappear. As a result of this, there is a minimal initial mass at the "background onset redshift" for the islands. We obtained the distribution function of the initial and final mass of the islands at different redshifts.

However, because ionized bubbles also formed within the large neutral islands, these bubbles-in-islands must be take into account. For this, we considered two barriers, the island barrier and the bubble barrier, at the same time. The former includes the effect of ionizing background at the surface of the island, while the latter does not. The bubbles embedded in an island were found by computing the first up-crossings over the bubble barrier after the random walks have down-crossed the island barrier at the host island scale and the volume fraction of the bubbles-in-island is obtained. We find that for a large island, a large fraction of its interior could be ionized.

The bubbles-in-island problem limited the applicability of this model, because in non-symmetrical cases, the presence of bubbles may break the island into small pieces, which would increase the exposed surface of the island. To address this problem, we applied a percolation criterion as an additional island barrier on large scales. Islands with large bubbles-in-island fractions are excluded, because in the real world where the bubbles are not spherical and concentric, these bubbles would have percolated through the island and broken it into smaller islands. Using the combined island barrier and excluding the ionized bubbles in the islands, the volume filling factor of neutral islands in the universe and the size distribution of the neutral islands were derived. Our island model applies to the large-scale structure of neutral regions in the linear regime, but it may be possible to account for the small-scale physics, such as the minihalo absorptions, by introducing a consuming term in the formula (e.g., Furlanetto & Oh 2005; Yue & Chen 2012).

At a given instant shortly after the isolation of islands, our model predicts that the size distribution of the islands has a peak of a few Mpc, depending on the model parameters. As the redshift decreases, the small islands disappear rapidly while the large ones shrink, but the characteristic scale of the islands does not change much. Eventually, all these large-scale neutral islands are swamped by ionization and only compact neutral regions such as galaxies or minihalos remain.

In our semi-empirical model of the ionizing background, the main absorbers of the ionizing photons are self-shielded LLSs. However, one needs to check to what extent the lower density neutral islands regulate the mean free path of the ionizing photons. The mean free path due to the existence of islands can be estimated by $\lambda^{\rm I}_{\rm mfp}(z) \sim 1/[\int \pi R_{\rm f}^2 (dn_{\rm f}/dM_{\rm f})\, dM_{\rm f}]$, where $R_{\rm f}$ and $dn_{\rm f}/dM_{\rm f}$ are the size and mass function of final host islands, respectively, at redshift z. We found that at $z = 6.9$, the mean free path of ionizing photons due to islands is $\lambda^{\rm I}_{\rm mfp} \sim 1.12$ physical Mpc as compared with that due to LLSs, $\lambda_{\rm mfp} \sim 0.30$ physical Mpc. At $z = 6.7$, $\lambda^{\rm I}_{\rm mfp} \sim 2.68$ physical Mpc as compared with $\lambda_{\rm mfp} \sim 0.38$ physical Mpc, while $z = 6.5$, $\lambda^{\rm I}_{\rm mfp} \sim 7.93$ physical Mpc as compared with $\lambda_{\rm mfp} \sim 0.48$ physical Mpc. Therefore, the mean free path of ionizing photons due to islands is always much larger than the mean free path due to LLSs and the effect of islands on the ionizing background is negligible compared with the effect of small-scale dense clumps. As the redshift decreases, the large-scale islands become less and less important in regulating the mean free path of ionizing photons. Considering the dominant contribution of LLSs to the IGM opacity, would they also contribute significantly to the neutral volume during the late era of reionization? The volume fraction of these LLSs can be estimated by $1 - F_{\rm V}(\Delta_{\rm crit})$, which is about 0.0062, 0.0046, and 0.0036 for $z = 6.9$, 6.7, and 6.5, respectively, much lower than the volume filling factor of the islands. Because of the much lower number density and larger size of islands, the mean free path due to islands is much larger than that due to LLSs, even though the volume filling fraction of islands is larger. Therefore, the majority of the neutral volume of the IGM is occupied by the islands, which is consistent with our model assumption, but the opacity of the IGM is dominated by the dense LLSs.

The results shown here are primarily qualitative; the quantitative predictions are dependent on our model assumptions and model parameters. Current observations have not yet been able to constrain such parameters effectively and they can be redshift dependent. Our model assumptions may also be too simplistic; for example, we may overpredict the number of large islands because they are more likely non-spherical and the ionizing background should have stronger effect on them as they have a larger surface area for the same volume. These uncertainties could be constrained in the future if the model predictions are compared with 21 cm and/or other observations and as the properties of ionizing sources, the evolution of neutral islands, and the intensity of the ionizing background become better known. We shall investigate the late reionization epoch by numerical simulations and compare it with the analytical models in subsequent works.

We deeply appreciate the insight of the referee and their constructive comments. We thank Jun Zhang, Jie Zhou, Hy Trac, and Renyue Cen for many helpful discussions. This work is supported by the Ministry of Science and Technology 863 project grant 2012AA121701, the NSFC grant 11073024, and the John Templeton foundation. Y.X. is supported by the China Postdoctoral Science Foundation and by the Young Researcher Grant of the National Astronomical Observatories, Chinese Academy of Sciences. Support for the work of M.S. was provided by NASA through an Einstein Postdoctoral Fellowship grant number PF2-130102 awarded by the Chandra X-ray Center, which is operated by the Smithsonian Astrophysical Observatory for NASA under contract NAS8-03060. Z.F. is supported by NSFC under grant 11173001 and 11033005.

REFERENCES

Alvarez, M. A., Busha, M., Abel, T., & Wechsler, R. H. 2009, ApJL, 703, L167
Barkana, R., & Loeb, A. 1999, ApJ, 523, 54
Battaglia, N., Natarajan, A., Trac, H., Cen, R., & Loeb, A. 2012a, ApJ, 776, 83
Battaglia, N., Trac, H., Cen, R., & Loeb, A. 2012b, ApJ, 776, 81
Bolton, J. S., & Haehnelt, M. G. 2013, MNRAS, 429, 1695
Bond, J. R., Cole, S., Efstathiou, G., & Kaiser, N. 1991, ApJ, 379, 440
Bouwens, R. J., Illingworth, G. D., Oesch, P. A., et al. 2011, ApJ, 737, 90
Bowman, J. D., & Rogers, A. E. E. 2010, Natur, 468, 796
Bradley, L. D., Trenti, M., Oesch, P. A., et al. 2012, ApJ, 760, 108
Bunde, A., & Havlin, S. 1991, Fractals and Disordered Systems (Berlin: Springer)
Calverley, A. P., Becker, G. D., Haehnelt, M. G., & Bolton, J. S. 2011, MNRAS, 412, 2543
Choudhury, T. R., & Ferrara, A. 2005, MNRAS, 361, 577
Choudhury, T. R., Haehnelt, M. G., & Regan, J. 2009, MNRAS, 394, 960
Cooray, A., & Sheth, R. 2002, PhR, 372, 1
D'Aloisio, A., & Furlanetto, S. R. 2007, MNRAS, 382, 860
Dawson, S., Rhoads, J. E., Malhotra, S., et al. 2007, ApJ, 671, 1227
Fan, X., Carilli, C. L., & Keating, B. 2006, ARA&A, 44, 415
Farahi, A., & Benson, A. J. 2013, MNRAS, 433, 3428
Finkelstein, S. L., Papovich, C., Ryan, R. E., et al. 2012, ApJ, 758, 93
Furlanetto, S. R., & Oh, S. P. 2005, MNRAS, 363, 1031
Furlanetto, S. R., Oh, S. P., & Briggs, F. H. 2006, PhR, 433, 181
Furlanetto, S. R., & Piran, T. 2006, MNRAS, 366, 467
Furlanetto, S. R., Zaldarriaga, M., & Hernquist, L. 2004, ApJ, 613, 1
Gallerani, S., Ferrara, A., Fan, X., & Choudhury, T. R. 2008a, MNRAS, 386, 359
Gallerani, S., Salvaterra, R., Ferrara, A., & Choudhury, T. R. 2008b, MNRAS, 388, L84
Gunn, J. E., & Peterson, B. A. 1965, ApJ, 142, 1633
Iliev, I. T., Shapiro, P. R., & Raga, A. C. 2005, MNRAS, 361, 405
Klypin, A., & Shandarin, S. F. 1993, ApJ, 413, 48
Komatsu, E., Smith, K. M., Dunkley, J., et al. 2011, ApJS, 192, 18
Kulkarni, G., Rollinde, E., Hennawi, J. F., & Vangioni, E. 2013, ApJ, 772, 93
Lacey, C., & Cole, S. 1993, MNRAS, 262, 627
Lorenzoni, S., Bunker, A. J., Wilkins, S. M., et al. 2013, MNRAS, 429, 150
Malhotra, S., & Rhoads, J. E. 2006, ApJL, 647, L95
McLure, R. J., Dunlop, J. S., Bowler, R. A. A., et al. 2013, MNRAS, 432, 2696
Mesinger, A., & Furlanetto, S. 2007, ApJ, 669, 663
Mesinger, A., McQuinn, M., & Spergel, D. N. 2012, MNRAS, 422, 1403
Miralda-Escudé, J., Haehnelt, M., & Rees, M. J. 2000, ApJ, 530, 1
Mo, H. J., & White, S. D. M. 1996, MNRAS, 282, 347
Musso, M., & Sheth, R. K. 2012, MNRAS, 423, L102
Musso, M., & Sheth, R. K. 2013, arXiv:1306.0551
Oesch, P. A., Bouwens, R. J., Illingworth, G. D., et al. 2012, ApJ, 759, 135
Oh, S. P., & Haiman, Z. 2003, MNRAS, 346, 456
Paciga, G., Albert, J. G., Bandura, K., et al. 2013, MNRAS, 433, 639
Paciga, G., Chang, T.-C., Gupta, Y., et al. 2011, MNRAS, 413, 1174
Pan, J., Wang, Y., Chen, X., & Teodoro, L. F. A. 2008, MNRAS, 389, 461
Paranjape, A., Lam, T. Y., & Sheth, R. K. 2012a, MNRAS, 420, 1648
Paranjape, A., Lam, T. Y., & Sheth, R. K. 2012b, MNRAS, 420, 1429
Paranjape, A., & Sheth, R. K. 2012, MNRAS, 419, 132
Park, H., Shapiro, P. R., Komatsu, E., et al. 2013, ApJ, 769, 93
Planck Collaboration, Ade, P. A. R., Aghanim, N., et al. 2013a, arXiv:1303.5076
Planck Collaboration, Ade, P. A. R., Aghanim, N., et al. 2013b, arXiv:1303.5084
Schaye, J. 2001, ApJ, 559, 507
Schenker, M. A., Stark, D. P., Ellis, R. S., et al. 2012, ApJ, 744, 179
Shapiro, P. R., Iliev, I. T., & Raga, A. C. 2004, MNRAS, 348, 753
Sheth, R. K., & Tormen, G. 2002, MNRAS, 329, 61
Sheth, R. K., & van de Weygaert, R. 2004, MNRAS, 350, 517
Shin, M.-S., Trac, H., & Cen, R. 2008, ApJ, 681, 756
Wyithe, J. S. B., & Bolton, J. S. 2011, MNRAS, 412, 1926
Yue, B., & Chen, X. 2012, ApJ, 747, 127
Zahn, O., Lidz, A., McQuinn, M., et al. 2007, ApJ, 654, 12
Zahn, O., Reichardt, C. L., Shaw, L., et al. 2012, ApJ, 756, 65
Zentner, A. R. 2007, IJMPD, 16, 763
Zhang, J., & Hui, L. 2006, ApJ, 641, 641
Zhou, J., Guo, Q., Liu, G., et al. 2013, RAA, 13, 373